



1 **A sea surface temperature reconstruction for the southern Indian**
2 **Ocean trade wind belt from corals in Rodrigues Island (19°S, 63°E)**

3

4 J. Zinke^{1,2,3}, L. Reuning⁴, M. Pfeiffer⁴, J. Wassenburg⁵, E. Hardman⁶, R. Jhangeer-Khan⁶,
5 Davies, G. R.⁷, C.K.C. Ng⁸, and D. Kroon⁹

6

7 ¹Department of Environment and Agriculture, Curtin University of Technology, Kent
8 Street, Bentley, WA6102, Australia

9 ²Australian Institute of Marine Science, Nedlands, WA 6009, Australia

10 ³School of Geography, Archaeology and Environmental Studies, University of
11 Witwatersrand, Johannesburg, South Africa.

12 ⁴Institute for Geology, RWTH Aachen, Wuellnerstrasse2, 52056 Aachen, Germany

13 ⁵Institute for Geosciences, Johannes-Gutenberg-University Mainz, Johann-Joachim-
14 Becher-Weg 21, D-55128 Mainz

15

16 ⁶SHOALS Rodrigues, Rodrigues, Mauritius

17 ⁷Department of Petrology, VU University Amsterdam, De Boelelaan 1085, 1081 HV
18 Amsterdam, Netherlands

19 ⁸Department of Medical Radiation Sciences, Curtin University of Technology, Kent
20 Street, Bentley, WA6102, Australia

21 ⁹University of Edinburgh, School of GeoSciences, The King's Buildings, West Mains
22 Road, Edinburgh EH9 3JW, UK.

23

24 **Correspondence to:** Jens Zinke, jens.zinke@gmail.com

25



26 **Abstract**

27 The western Indian Ocean has been warming rapidly over the past decades and this has
28 adversely impacted the Asian Monsoon circulation. It is therefore of paramount
29 importance to improve our understanding of links between Indian Ocean Sea Surface
30 Temperature (SST) variability, climate change, and sustainability of reef ecosystems.
31 Here we present two monthly-resolved coral Sr/Ca records (Totor, Cabri) from Rodrigues
32 Island (63°E, 19°S) in the south-central Indian Ocean trade wind belt, and reconstruct
33 SST based on the linear relationship with the Sr/Ca proxy. The records extend to 1781
34 and 1945, respectively. We assess the reproducibility of the Sr/Ca records, and potential
35 biases in our reconstruction associated with the orientation of corallites. We quantify
36 long-term SST trends and identify interannual relationships with the El Niño-Southern
37 Oscillation (ENSO) and the Pacific Decadal Oscillation (PDO). We conclude that careful
38 screening for diagenesis and orientation of corallites is of paramount importance to assess
39 the quality of Sr/Ca-based SST reconstructions. Our proxy records provide a reliable SST
40 reconstruction between 1945 and 2006. We identify strong teleconnections with the
41 ENSO/PDO over the past 60 years, eg. warming of SST during El Niño or positive PDO.
42 We suggest that additional records from Rodrigues Island can provide excellent records
43 of SST variations in the southern Indian Ocean trade wind belt and teleconnections with
44 the ENSO/PDO on longer time scales.

45

46 **1 Introduction**

47 The Indian Ocean has been warming steadily over the past century with the western
48 portion of the basin having experienced an increase in SST of up to 1.2°C over the past



49 60 years (Koll Roxy et al., 2014). The Indian Ocean has also taken up a large amount of
50 heat in its interior during the recent 15 years when global SST increased at a smaller rate
51 as compared to previous decades (Lee et al., 2015). The strong Indian Ocean warming
52 over the past century is thought to have contributed to a decreasing land-sea thermal
53 contrast with the Indian subcontinent affecting monsoon rainfall and might have played a
54 major role for the decrease in East African rainfall between March to May in recent
55 decades (Funk et al., 2008; Koll Roxy et al., 2015). The western Indian Ocean warming
56 has also been shown to follow closely anthropogenic radiative forcing over the past
57 century (Funk et al., 2008; Alory et al., 2009; Koll Roxy et al., 2015). Furthermore, the
58 western Indian Ocean warmed significantly during past El Niño events with the 1997/98
59 event having caused widespread coral bleaching and mortality. It is therefore of
60 paramount importance to improve our understanding of links between Indian Ocean SST
61 variability, global climate change, and sustainability of reef ecosystems. Yet, long-term
62 observational records of Indian Ocean SST are sparse and are thought to be only reliable
63 after the 1960's (Tokinaga et al., 2012). To overcome the limitations of the short
64 observational record, paleoclimate records of past SSTs can be generated to provide
65 insight into long-term SST changes and interannual to decadal variability.

66 Paleoclimate reconstructions of SST from massive corals have provided
67 invaluable records for past SST trends and interannual to decadal variability in the
68 western Indian Ocean (Charles et al., 1997; Cole et al., 2000; Cobb et al., 2001; Pfeiffer
69 et al., 2004, 2009; Pfeiffer & Dullo, 2006; Nakamura et al., 2009; Crueger et al., 2009;
70 Grove et al., 2013; Zinke et al. 2008, 2009, 2014). Massive corals, such as *Porites* spp.,
71 can grow for centuries and grow at a rate between 0.5 and 2 cm yr⁻¹. Therefore, down-



72 core sampling of massive corals yields an in situ SST time series of monthly resolution.
73 As the coral precipitates its skeleton, trace elements and stable isotopes are incorporated
74 at different concentrations, relative to Ca, in relation to changing SSTs (Felis and Pätzold,
75 2003). Both, the Sr/Ca ratio and $\delta^{18}\text{O}$ composition of the coral aragonite were shown to
76 be reliable paleo-thermometers, whereby a negative relationship exists with SST (Alibert
77 and McCulloch, 1997; Pfeiffer & Dullo, 2006; DeLong et al., 2012). A compilation of
78 Sr/Ca-SST calibrations for *Porites spp.* revealed a mean Sr/Ca relationship with SST of -
79 0.061mmol/mol/1°C SST increase (Corrège, 2006). Since Sr has a long oceanic residence
80 time, skeletal Sr/Ca is assumed to mainly reflect SST variability. The quality and
81 accuracy of paleo-thermometers strongly depends on optimal sampling of the major
82 growth axes (De Long et al., 2012). Furthermore, diagenetic alterations of coral aragonite
83 can lead to errors in SST reconstructions and need to be excluded by specific analysis
84 (McGregor and Gagan, 2003; McGregor and Abram, 2008; Sayani et al., 2011; Smodej et
85 al., 2015).

86 Currently, none of the coral proxy records from the western Indian Ocean cover
87 the south-central Indian Ocean basin in the heart of the trade wind system. Furthermore,
88 all proxy records of interest for the trade wind belt are based on oxygen isotopes with the
89 exception of two Sr/Ca ratio records covering 1952 to 2008 from St. Marie Island off
90 East Madagascar (Grove et al., 2013). The latter provided mixed results with
91 discrepancies in terms of the long-term SST trend estimates due to confounding effects of
92 coral calcification in at least one of the cores (Grove et al., 2013). A coral oxygen isotope
93 record from Reunion Island (21°S, 55°E; Mascarene Islands) located approximately
94 230km to the southwest of Mauritius spans the period 1832 to 1994 and is the longest for



95 the subtropical region off East Madagascar (Pfeiffer et al., 2004). Pfeiffer et al. (2004)
96 showed evidence that the La Reunion coral dominantly recorded past variations in the
97 salinity anomalies associated with transport changes of the South Equatorial Current. The
98 proxy record showed decadal anomalies that were opposite to those of SST. Crueger et al.
99 (2009) showed close linkages of the salinity, SLP and SST signal associated with the
100 Pacific Decadal Oscillation (Mantua et al., 1997) in coral records from Reunion and Ifaty
101 (SW Madagascar), respectively. Two coral oxygen isotope records from the Seychelles
102 located in the tropical western Indian Ocean (5°S, 54°E) were interpreted as an excellent
103 record of past Southwest Monsoon SST changes and showed strong correlations with air
104 temperatures over India between 1847 to 1994 (Charles et al., 1997; Pfeiffer & Dullo,
105 2006). Both, the Reunion and Seychelles records showed strong correlations with the El
106 Nino-Southern Oscillation on interannual and decadal time scales (Pfeiffer & Dullo,
107 2006).

108 Here, we aim to reconstruct past SSTs from Sr/Ca ratios in two coral cores
109 obtained from Rodrigues Island (19°S, 63°E) located 500 km to the North-East of
110 Mauritius within the trade wind belt of the south-central Indian Ocean. We assess the
111 reproducibility of the Sr/Ca proxy from two different locations, their long-term trends and
112 interannual variability related to the El Nino-Southern Oscillation.

113

114 **2 Regional setting and climate**

115 Rodrigues (63°E, 19°S) is a small volcanic island in the southern Indian Ocean, about
116 619 km east of Mauritius (Fig. 1). It is part of the eastern edge of the Mascarene Plateau
117 that is made up of Lower Tertiary basalts (Mart 1988) that formed by a seaward flow of



118 lava, which has been eroded by hydrodynamic forces, and biological and chemical
119 processes (Turner and Klaus, 2005). Rodrigues has a surface area of about 119 km², with
120 a maximum altitude of 396 meter above sea level and is surrounded by a nearly
121 continuous fringing reef, which form an almost continuous band measuring
122 approximately 90km in length (Turner and Klaus, 2005; Lynch et al. 2002). The reef
123 encloses a shallow lagoon, which, at 240km², is twice the area of the island itself. The
124 maximum tidal range is approximately 1.5m, and since the average water depth in the
125 lagoon is less than 2m, some areas are exposed at low spring tides. The water depth
126 immediately beyond the reef slopes is usually within the range of 10m to 30m. The island
127 has three major channels, one dredged channel for the main harbour at Port Mathurin in
128 the north, and natural channels in the south near Port Sud Est and in the East at St
129 Francois. Several small passes are also found at intervals around the reef (Turner and
130 Klaus, 2005).

131 The water surrounding Rodrigues is supplied by the South Equatorial Current (SEC)
132 (New et al. 2007) which is a broad east to west current between 10° and 20° S in the
133 Indian Ocean driven by the southeast trade winds (Schott and McCreary, 2001). The
134 southern part of the SEC water flows in several directions, alongside Rodrigues in
135 southwest and southeast direction, and westward to Mauritius (New et al. 2007).

136 Rodrigues has a relatively dry climate and evaporation exceeds precipitation on the
137 annual mean. Yearly precipitation is ~1000 mm with most precipitation from January to
138 April related to the position of the Inter Tropical Convergent Zone (ITCZ). Between
139 November and March, the Southern Indian Ocean is affected by tropical cyclones, as a
140 result of warm SSTs and a strong convergence between northeast and southeast trades.



141 Rodrigues experiences two to sixteen cyclones per year, of which 2.5 are extreme: with
142 winds of 280 km/h and waves that reach 100 m inland and 2 m above sea level. They
143 usually last five to ten days (Turner and Klaus, 2005).

144 SST was monitored *in situ* by a CTD 150m offshore from the northern fringing reefs
145 at Totor between 2002 to 2006 (Fig. 2a). Maximum SST are recorded between December
146 to March ($28.6 \pm 0.5^{\circ}\text{C}$) and minimum SST between July to September ($22.4 \pm 0.27^{\circ}\text{C}$).
147 Annual mean SST is $25.49 \pm 0.24^{\circ}\text{C}$ with a seasonal amplitude of $6.22 \pm 0.68^{\circ}\text{C}$ (Fig. 2a).

148 Air temperatures are recorded by the WMO weather station located at the northern
149 coast of Rodrigues since 1951 and are available at <http://climexp.knmi.nl/>. The most
150 recent years between 1997 and 2007 have been provided by the Rodrigues
151 Meteorological Office (Fig. 2b). The warmest months are December to March ($31.2 \pm$
152 0.3°), the coldest months are July to September ($24.2 \pm 0.3^{\circ}$). Yearly average air
153 temperature is $27.49^{\circ}\text{C} \pm 0.31^{\circ}\text{C}$ with a yearly amplitude of about $7 \pm 0.79^{\circ}\text{C}$.

154

155 **3 Materials and Methods**

156 Two cores were drilled from massive, dome-shaped *Porites* sp. and *Porites lobata*
157 at the northern reef sites Totor (S19°67062; E63°42923) and Cabri (S19°667171,
158 E63°43.4423), respectively (Fig. 1; Table 1). The size of the coral colonies at Totor is
159 ~2.5m and that of Cabri is ~4m in height. Both colonies were healthy and showed no
160 signs of disease or dead surfaces at the time of drilling. The 220cm long core Totor was
161 obtained in August 2005 from the forereef slope of the northern fringing reef facing the
162 open ocean with the top of the colony at 4m water depth. The 180cm long core Cabri was
163 obtained in March 2007 growing in 3m water depth about 1km to the northeast of Totor



164 from the outer fringing reef. The site Cabri is more exposed to trade winds as compared
165 to Totor which is more sheltered.

166 A commercially available pneumatic drill driven by scuba tanks was used to
167 extract cores along the central growth axis, with a diameter measuring 4 cm. Cores were
168 sectioned into 7 mm thick slabs, rinsed several times with demineralised water, blown
169 with compressed air to remove any surficial particles and dried for more than 24 hours in
170 a laminar flow hood. Growth laminae were visualised by X-radiograph-positive prints,
171 and the growth axis of the coral slab was defined as the line normal to these laminae
172 (Appendix Fig. 7 and 8). Coral densities (g/cm^3) were calculated by analysing digital X-
173 rays using the program CoralXDS and densitometry (Helmle et al., 2011; Carricart-
174 Ganivet et al., 2007), calcification rate ($\text{g/cm}^2 \text{yr}^{-1}$) by multiplying density with extension
175 rate. The annual extension rates (cm yr^{-1}) were calculated by measuring the distance (cm)
176 between density minima using the program CoralXDS. With a diamond coated drill
177 mounted on top of a movable frame, samples were taken every 1 mm parallel to the
178 growth axis, equivalent to approximately monthly resolution.

179 A combination of X-ray images, X-ray diffraction (XRD), light and scanning
180 electron microscopy (SEM) with Energy Dispersive X-Ray Spectrometer (EDS) was used
181 to investigate possible diagenetic alteration from cores Totor and Cabri. All coral slabs
182 from cores Toto and Cabri were initially screened for diagenetic alterations using X-ray
183 images (Figs. A7, A8). Corals that showed an annual density banding without anomalous
184 high or low density patches were selected for further study and considered free from
185 obvious diagenetic alteration. Representative samples were chosen from both cores based
186 on the X-ray images for SEM, thin-section and XRD analysis. Additional samples were



187 selected after geochemical analysis targeting intervals with unusually high or low Sr/Ca
188 ratios. The powder-XRD diffractometer at RWTH Aachen University was calibrated to
189 detect and quantify very low calcite contents (detection limit $\sim 0.2\%$) following the
190 method described by Smodej et al. (2015). In addition, the 2D-XRD system Bruker D8
191 ADVANCE GADDS was used for XRD point-measurements directly on the coral slab
192 with a spatial resolution of ~ 4 mm and a calcite detection limit of $\sim 0.2\%$ (Smodej et al.,
193 2015). A 2-dimensional detector allows the simultaneous data collection over a large 2θ
194 range, which reduces the counting time to 10 min for each sampling spot. The coral is
195 mounted on a motorized XYZ-stage and the position of each sample spot is controlled by
196 an automated laser-video alignment system. Multiple sample points can be predefined
197 and measured automatically. This method was used to test for the presence of secondary
198 calcite along the geochemical sample traces of both corals.

199 Sr/Ca ratios were measured at the University of Kiel with a simultaneous
200 inductively coupled plasma optical emission spectrometer (ICP-OES, Spectro Ciros CCD
201 SOP; Zinke et al., 2014). Approximately 0.5mg of coral powder are dissolved in 1.00 ml
202 0.2M HNO₃. Prior to analysis, this digest solution is diluted with 0.2M HNO₃ to a final
203 concentration of approx. 8ppm Ca. An in-house coral powder standard (Mayotte) was
204 prepared in an analogue way and used as consistency standard, being re-analyzed after
205 every six samples. The international reference material JCp-1 (coral powder) was
206 analyzed with every sample batch. All calibration solutions are matrix-matched to 8 ppm
207 Ca. Strontium and Ca are measured at their 407 and 317 nm emission lines. Our intensity
208 ratio calibration strategy combines the techniques described by de Villiers et al. (2002)



209 and Schrag (1999). Analytical precision of Sr/Ca determinations as estimated from
210 replicate measurements of unknown samples is 0.15% or 0.01 mmol/mol (1sigma).

211 The coral core chronologies were developed based on the seasonal cycle of Sr/Ca.
212 We assigned the coldest month (either August or September) to the highest measured
213 Sr/Ca ratio in any given year, according to both *in situ* SST and grid-SST (Extended
214 reconstructed SST; Smith et al., 2008). We then interpolated linearly between these
215 anchor points to obtain age assignments for all other Sr/Ca measurements. In a second
216 step, the Sr/Ca data were interpolated to 12 equidistant points per year to obtain monthly
217 time series using AnalySeries 2.0 (Paillard et al., 1996). This approach creates a non-
218 cumulative time scale error of 1 - 2 month in any given year, due to interannual
219 differences in the exact timing of peak SST. The monthly interpolated Sr/Ca time series
220 were cross-checked with the chronologies from coral XDS to reveal the timing of high
221 and low density banding. High density bands in both corals formed in summer (low
222 Sr/Ca) of any given year.

223

224 **4 Historical SST data**

225 Historical SST data collected primarily by ships-of-opportunity have been summarised
226 in the comprehensive ocean atmosphere data set (ICOADS) to produce monthly averages
227 on a 2°x2° grid basis (Woodruff et al., 2005). In the grid that includes Rodrigues Island
228 the data are extremely sparse (<http://climexp.knmi.nl>). We therefore extracted SST from
229 extended reconstructed SST (ERSST version 3b/v4; Smith et al., 2008), also based on
230 ICOADS data, which uses sophisticated statistical methods to reconstruct SST in time of
231 sparse data. From ERSST, we extracted data in the 2°x2° grid centred at 61-63°E, 19-



232 21°S (Table A1). Between 2002 and 2006 (*in situ* data coverage) ERSST version 3b
233 shows a yearly average of about $25.57\text{C} \pm 0.19\text{C}$ with a yearly amplitude of $5.14 \pm$
234 0.39C (Smith et al., 2008). The warmest months are February and March with a SST of
235 $28.29\text{C} \pm 0.4\text{C}$, the coldest months are August and September with a SST of $23.15\text{C} \pm$
236 0.13C .

237 Furthermore, we used Met Office Hadley Centre's sea ice and sea surface temperature
238 (HadISST) data for the grid 62-63°E, 19-20°S (Rayner et al., 2003; Kennedy et al., 2011;
239 Table A1). HadISST temperatures are reconstructed using a two-stage reduced-space
240 optimal interpolation procedure, followed by superposition of quality-improved gridded
241 observations onto the reconstructions to restore local detail. Since January 1982, SST
242 time series for HadISST use the optimal interpolation SST (OISST; $1^\circ \times 1^\circ$), version 2
243 (Reynolds et al., 2002) that includes continuous time series of satellite-based SST
244 measurements. We also extracted Advanced Very High Resolution Radiometer
245 (AVHRR) SST at $0.25^\circ \times 0.25^\circ$ resolution (Reynolds et al., 2007) from 1985 to 2006
246 which is also used by NOAA's coral reef watch. AVHRR SST for Rodrigues between
247 2002 and 2006 (*in situ* data coverage) provided from NOAA at $0.25^\circ \times 0.25^\circ$ resolution
248 (Reynolds et al., 2007) shows a yearly average of $25.4 \pm 0.11\text{C}$ with a yearly amplitude
249 of $5.9 \pm 0.58\text{C}$. Warmest SSTs are observed between January and March ($28.65 \pm$
250 0.44C) and coolest SST between July to September ($22.75 \pm 0.21\text{C}$).

251 SST from the $5^\circ \times 5^\circ$ HadSST3, the most sophisticated bias-corrected SST data to
252 date, were downloaded for the region 60-65°E, 15-20°S (Kennedy et al., 2011; Appendix
253 Table 1). Yet, HadSST3 contains data gaps throughout the record due to strict quality
254 control. SST is reported as anomalies relative to the 1961 to 1990 mean climatology.



255 In addition, we extracted 5°x5° night-time marine air temperature data from
256 HadMAT1 and HadNMAT2 datasets (Kent et al., 2013). HadNMAT2 contains data gaps
257 throughout the record due to strict quality control. Night-time marine surface air
258 temperature is highly correlated with SST but free of the biases introduced by changes in
259 SST measurement techniques (Tokinaga et al., 2012).

260

261 **5 Results**

262 **5.1 Coral growth parameters**

263 The average growth rate of the corals Totor (224 years) and Cabri (130 years)
264 over all years of growth were $9.82 \pm 0.19 \text{ mm y}^{-1}$ and $11.79 \pm 0.25 \text{ mm y}^{-1}$, respectively
265 (Table 1; Fig. A1). The Cabri core shows a growth disturbance at 1907 that led to partial
266 colony death. This is confirmed by three additional cores taken from this colony at
267 different angles which all showed the mortality event marked by a dead surface pre-
268 dating ~1907. This lower core section is overprinted by diagenesis and it is therefore not
269 suitable for climate studies or to determine density and calcification rates.

270 Extension rate of the Cabri coral shows no long-term trend, yet shows high
271 interannual and decadal variability (Fig. A1). The same holds for calcification rates. Both
272 extension and calcification show marked interannual oscillation in the recent 10 years.
273 Skeletal density shows multidecadal oscillations with high densities between 1907 and
274 1935, the early 1940's, between 1958 and 1966 and 1980 and 2006, with lower densities
275 in between (Fig. A1).

276 The Totor core shows a similar decadal and interannual variability in extension
277 and calcification compared to the Cabri core for the period of overlap between 1877 and



278 2005 (Fig. A1). The fit is less optimal between 1877 and 1907 due to the dead surface in
279 Cabri that has obscured density banding. No significant trend is observed in both
280 extension and calcification rates over the entire record length. Skeletal density differs
281 between the two cores. The Totor core shows multi-decadal cycles in density
282 superimposed on a decreasing trend and larger magnitude density anomalies compared to
283 the Cabri core. Between 1960 and 2005 both density profiles agree well in terms of
284 decadal variability, both showed a significant drop since the late 1960's and recovery
285 thereafter. However, the low density period in the Totor core lasted several years longer.

286

287 **5.2 Seasonality, trends and variability in Sr/Ca and instrumental SST time series**

288 For the period of overlap between both cores (1945 to 2005) there is a between
289 colony offset in mean Sr/Ca of 0.0242 mmol/mol. Both cores show a distinct seasonality
290 in Sr/Ca throughout their record length (Fig. 3). The seasonality in the Totor core
291 (0.283 ± 0.049 mmol/mol) is on average slightly higher compared to the Cabri core
292 (0.238 ± 0.055 mmol/mol), yet both overlap within 1σ .

293 To eliminate the offset between Sr/Ca time series we calculated Sr/Ca anomalies
294 by subtracting their mean relative to the 1961 to 1990 reference period (Figure 3). We
295 subsequently calculated relative changes in SST based on the established empirical
296 relationship of -0.0607 mmol/mol per 1°C derived from >30 published Sr/Ca calibrations
297 (Corrège, 2006). A composite coral temperature record was then constructed by (1)
298 converting each proxy record to temperature units, (2) calculating the arithmetic mean of
299 the coral records from each site, and (3) averaging the mean records from both sites.



300 Between 1945 and 2006 both cores indicate higher Sr/Ca anomalies (a period of
301 cooling) that started in the mid 1950's and lasted until the early 1970's. Both cores show
302 a pronounced trend to more negative Sr/Ca values (warming) starting in the 1970's and
303 reduced seasonality in that period (Fig. 3). After 1984 Sr/Ca in the Cabri core further
304 decreases (warms) while core Sr/Ca in the Totor core has no trend. The detrended Sr/Ca
305 time series indicated that both cores show similar decadal oscillations between 1945 and
306 2005 (not shown). This highlights that the long-term trend estimates after 1984 need to be
307 viewed with caution.

308 The Sr/Ca time series in the Totor core extends to 1781. Marked negative Sr/Ca
309 anomalies (warmer) are observed during the first half of the 20th century centered at
310 1918/19, 1936-41 and in the period 1947-1951 that exceed anomalies in the 1961 to 1990
311 reference period. Sr/Ca anomalies between 1850 and 1900 are higher (cooler) while
312 decadal periods with lower (warmer) Sr/Ca are observed between 1781 and 1850 relative
313 to 1961 to 1990. The long-term trend in Sr/Ca anomalies between 1781 and 2005
314 converted to SST indicated an overall warming of 0.44°C.

315 The composite Sr/Ca time series displays interannual and decadal variability
316 throughout the record between 1781 and 2006. The anomaly around 1918/19 is the lowest
317 (warmest) of the entire record length. In general, Sr/Ca anomalies during the 20th century
318 are lower (warmer) than between 1850 and 1900, while anomalies between 1781 and
319 1850 reach similar levels relative to the period 1961 to 1990 for several decades with
320 short-lived excursions to higher (cooler) anomalies. The long-term trend in Sr/Ca
321 anomalies between 1781 and 2006 converted to SST indicated an overall warming of
322 0.37°C.



323

324 **5.3 Calibration/validation of coral Sr/Ca-SST**

325 We calibrated the coral Sr/Ca from both cores with *in situ* SST, ERSSTv.3b and
326 AVHRR SST for the period 2002 to 2006 using the minima and maxima in any given
327 year, as well as monthly values with AVHRR SST for 1981 to 2006 (Fig. 4; Tab. A2).
328 The slopes of the ordinary least squares regressions vary between -0.0384 to -0.0638
329 mmol/mol per 1°C (Tab. A2). The lowest slopes are obtained with *in situ* SST and the
330 highest with ERSSTv.3b (Tab. A2). We reconstructed absolute SST for the period of
331 overlap with *in situ* SST from 2002 to 2006 from both coral cores (Fig. 4). The Sr/Ca-
332 SST in the Totor core shows the best fit with *in situ* SST in terms of the seasonal
333 amplitude. The Sr/Ca-SST in the Cabri core overestimates the winter SST of 2002 and
334 2005, yet agrees well for 2003 and 2004 (Fig. 4). However, taking into account the
335 uncertainties (measurement error, regression error) around absolute SST from Sr/Ca for
336 Cabri and Totor of 1.23°C and 1.05°C (1 σ), respectively, the coral data agree with *in situ*
337 SST within the 1 σ uncertainty.

338 To eliminate large errors associated with absolute SST reconstructions from coral
339 Sr/Ca we calculated relative changes in SST for the composite coral temperature record
340 relative to the 1961 to 1990 mean based on the established empirical relationship of -
341 0.0607 mmol/mol per 1°C derived from >30 published Sr/Ca calibrations (Corrège,
342 2006). This slope is well within the range of our regressions based on a variety of SST
343 datasets (Tab. A2). We use a conservative estimate for the uncertainty around relative
344 SST changes based on the difference between lower (-0.04) and upper slope (-0.084)



345 estimates from these regression equations, thus ± 0.02 mmol per 1°C or $\pm 0.33^{\circ}\text{C}$
346 (following Gagan et al., 2012; Tab. A2).

347 We validated the coral derived annual mean SST reconstruction against local Air
348 Temperature (AT), ERSSTv3b, ERSST4, HadISST, HadSST3 HadMAT1 and
349 HadNMAT2 for the period 1951 to 2006 (Figure 5; Figs. A4 to A6; See Supplementary
350 Tables 1-24 for mean annual correlations). The composite coral SST record clearly
351 follows instrumental SST in the grid box surrounding Rodrigues Island while the best fit
352 is obtained with local Rodrigues AT. Discrepancies with gridded SST products are
353 observed between 1951 and 1955. However, AT agrees with coral composite SST in that
354 period, yet not with core Cabri which tracks grid-SST between 1951 and 1955. However,
355 taking into account the uncertainty of $\pm 0.33^{\circ}\text{C}$ based on the regression error, coral
356 composite SST agrees with gridded SST within 1σ .

357 For the period 1951 to 2005, we used AT, ERSSTv3b, ERSST4, HadISST,
358 HadSST3, HadMAT1 and HadNMAT2 to validate trends in annual mean coral Sr/Ca-
359 SST anomalies (Fig. 5, 6). The long-term trends in Sr/Ca-derived SST anomalies for the
360 period 1951 to 2005 for Cabri and Totor converted to SST, using the published Sr/Ca-
361 SST relationship of $-0.0607\text{mmol/mol per }1^{\circ}\text{C}$, indicate a warming of $1.38\pm 0.39^{\circ}\text{C}$ and
362 cooling of $-0.49\pm 0.41^{\circ}\text{C}$, respectively. The composite Sr/Ca anomaly time series for 1951
363 to 2005 display a warming trend of $0.44\pm 0.37^{\circ}\text{C}$. The uncertainty for the trend estimates
364 in coral Sr/Ca SST is calculated from the square root of the sum of squares of the
365 regression error and the error in the slope of the Sr/Ca-SST relationship. Instrumental
366 SST indicate a warming trend of $0.61\pm 0.13^{\circ}\text{C}$ for HadISST, $0.72\pm 0.11^{\circ}\text{C}$ for ERSST3b
367 ($0.86\pm 0.12^{\circ}\text{C}$ for ERSST4) and $0.78\pm 0.12^{\circ}\text{C}$ for HadSST3. Air Temperature at



368 Rodrigues weather station recorded a warming trend of $0.46 \pm 0.17^\circ\text{C}$. All trends are
369 significant at the 2% level with the exception of the negative trend in Sr/Ca SST
370 anomalies in the Totor core which is not significant.

371 For the pre-1945 period we used ERSSTv3b, HadSST1 and HadSST3 to validate
372 annual mean coral Sr/Ca-SST back to 1854 and 1870, respectively (Figure 6). We stress
373 that the number of SST observations in the ICOADS SST database is extremely sparse
374 for our region (Fig. A2). However, the composite coral SST record tracks SST variations
375 for most of the past 150 years (Figure 6). The composite coral SST time series,
376 essentially the time series of core Totor, displays higher SST anomalies compared to all
377 gridded SST reconstructions in the 1850's, between 1916-1921, 1936-1941 and 1948-
378 1951 and lower SST anomalies for brief periods between 1850 and 1890. In general, the
379 coral composite SST is a valid reconstruction for the region surrounding Rodrigues Island
380 with the possible exception of 1854-1860, 1916-1921, 1936-1941 and 1948-1951 (Figure
381 6).

382 Largest discrepancies between grid-SST (starting from year 1854) and coral SST
383 reconstructions are found for core Totor with warm anomalies in the periods 1854-1860,
384 1916-1921, 1936-1941 and 1948-1951 (Figure 6). Interestingly, the correlation between
385 Totor Sr/Ca-SST, which dominates the coral composite time series pre-1945, has
386 significant correlations with HadSST3 ($r=0.24$; $p=0.05$; $N=65$) and HadNMAT2 ($r=0.3$;
387 $p=0.014$; $N=64$) observational time series only. The cool bias in coral derived SST
388 between 1882 and 1887 (slab 7) is most probably related to diagenetic alterations, but
389 none of the anomalously warm periods can be explained by diagenesis (see next section).
390 We assessed the orientation of corallites to the coral slab surface to test for sampling



391 artifacts that might have altered our Sr/Ca data which we summarized in Tables 2 and 3,
392 illustrate in Figure 7 and discuss in section 6.1. Most anomalous warm periods show sub-
393 optimal orientation of sampling path with corallites at an angle to the slab surface (see
394 6.1).

395

396 **5.4 Diagenetic tests for alterations of Sr/Ca profiles**

397 Representative samples for diagenetic screening with XRD, SEM and light
398 microscopy were identified on the coral slabs using the X-radiographs. Additionally,
399 intervals with presumably anomalous proxy values (warm or cold anomalies) were
400 analyzed with the same methods. Ten thin-sections, six SEM samples, ten powder-XRD
401 and thirteen spot-2D-XRD samples were analyzed from coral core Totor (Fig. 8). For
402 coral core Capri, seven thin-sections, one powder-XRD and six 2D-XRD samples were
403 analyzed. Neither powder nor spot-XRD analysis detected any calcite. Thin-section
404 analysis indicates a growth break within slab 12 that is also apparent in the radiograph
405 (Fig. 8; Fig. A7). Close to this break the coral is strongly affected by bioerosion and
406 encrustation by red algae (Fig. 8ef). However, the sampling transect for geochemical
407 analysis excluded this area and is therefore not affected by diagenesis (Fig. 8f).
408 Combined SEM, EDS and XRD analysis shows low amounts of patchy distributed
409 isopachous (~2µm) fibrous aragonite cement in slabs Totor 6 (1916-1921), 7 (1882-1887)
410 and 11 (~ 1809).

411 Aragonite cement should lead to higher Sr/Ca values and lower reconstructed
412 temperatures (Hendy et al., 2007). An interesting outcome is that the observed diagenesis
413 is not able to explain the Sr/Ca ratios except for the slab Totor 7. Here the observed



414 aragonite cement fits to relatively high Sr/Ca values resulting in a cold anomaly. No
415 anomalously high Sr/Ca ratios are associated with the patchy aragonite cements in slabs 6
416 and 11. Instead slabs 6 and 11 are characterized by low Sr/Ca ratios resulting in relatively
417 warm reconstructed temperatures. All other samples from the slabs Totor 3, 4, 8, 9 and 10
418 are devoid of diagenetic alteration. In summary, an influence of diagenesis on the proxy
419 record and resulting SST reconstructions can only be assumed for sample Totor 7 (years
420 1882-1887). Core Cabri showed only localized (single month) positive Sr/Ca anomalies
421 (cool SST bias). Thin-section and XRD analysis did not indicate any diagenetic
422 alteration, but the coral locally contained aragonitic sediment partially filling pore spaces
423 (Tab. 3). This aragonitic sediment potentially could have caused the isolated Sr/Ca peaks.
424 These individual data points were omitted from further analysis.

425

426 **5.5 Large scale teleconnections on interannual time scales**

427 For the period of most reliable data coverage between 1951 and 2006, the
428 detrended coral composite and Cabri Sr/Ca-SST records shows positive correlations for
429 austral summer and annual means with Indian Ocean wide SST and a positive correlation
430 with the central and eastern Pacific SST typical for the spatial ENSO and PDO pattern
431 (Figure 9; Supplementary Tables 24-25). We used HadISST (1870 and 2006) and
432 HadMAT1 to evaluate the long-term spatial correlation pattern (Figs. A3 to A5). A similar
433 pattern emerged as for the period 1951 to 2006, yet of weaker magnitude across the
434 Pacific and confined to the southwestern Indian Ocean. We broke down the correlations
435 into 30 year segments starting in 1870 to test if the correlation changes throughout the
436 past 136 years. The ENSO/PDO pattern for austral summer is strong in the periods 1870-



437 1900, 1961-1990 and 1971-2006 (Fig. A3). Between 1900 and 1930 the correlation is not
438 significant. The large-scale teleconnections with SST are stronger for the Cabri Sr/Ca-
439 SST time series after 1945 (Figs. A4, A5), while core Totor has weaker and statistically
440 non-significant correlations in that period. This indicates that the Cabri time series is
441 more reliable for the recent 60 years for monthly averages and annual means and shows
442 the strongest correlations across the Indo-Pacific (Fig. 9; Figs. A4, A5; Supplementary
443 Tables 25, 26).

444 For detrended mean annual time scales (July-June) and austral summer (JFM) the
445 Cabri SST record shows a positive correlation with southern Indian Ocean SST along a
446 southeast to northwest band stretching along the trade wind belt (Figure 9d-f; Fig. A4).
447 The correlation with the southern Indian Ocean trade wind belt remains stable over
448 different record length and is most pronounced post 1971. We also find positive
449 correlations with the Bay of Bengal and the Maritime Continent throughout the past 60
450 years. We find positive correlations with the eastern Pacific SST and negative
451 correlations with the northern Pacific along 40°N and stretching between 160°E and
452 150°W. The SST pattern mimics part of the typical spatial ENSO and PDO pattern across
453 the Indo-Pacific (Mantua et al., 1997; McPhaden et al., 2006).

454

455 **6 Discussion**

456 **6.1 Diagenesis, orientation of corallites and potential biases in Sr/Ca derived SST**

457 Diagenesis could be excluded as a major cause of discrepancies between coral
458 SST and grid-SST. For core Totor, only for the period between 1882 and 1887 we have to
459 assume that diagenesis caused a cool bias on our coral SST reconstruction (Figure 8).



460 Core Cabri showed only localized positive Sr/Ca anomalies (cool SST bias) most
461 probably caused by aragonitic sediment trapped within growth framework pores. These
462 samples have been removed before interpolation. Having excluded diagenesis for most of
463 the record, we assessed sampling biases due to changes in the orientation of growth axes
464 and positioning of corallites to the slab surface. De Long et al. (2012) showed clear
465 evidence for warm or cool biases in coral Sr/Ca-SST reconstructions caused by
466 suboptimal orientation of corallites in corals from New Caledonia. We have adopted a
467 similar approach to test for sampling biases in our two cores (Table 2 & 3). We found
468 that core Totor contained areas where a sampling bias could explain anomalous Sr/Ca-
469 derived SST. The warm anomaly between 1916 and 1921 with its peak values in 1919
470 stands out as the largest single anomaly in the record. However, diagenesis cannot
471 explain the warm anomalies. The growth rates and Sr/Ca seasonality for all years
472 between 1916 and 1921 are not anomalous and close to the average seasonality from *in*
473 *situ* SST data. The orientation of the corallites is mostly optimal (parallel to slab surface)
474 to the surface. However, for the years 1916 to 1921 we recognized an interval with
475 bundles of oblong corallites where our sampling transects switched from optimal to
476 suboptimal growth orientation. De Long et al. (2012) showed that warm biases were often
477 caused by corallites orientated at an angle or oblong to the slab surface and where growth
478 orientation had changed. These suboptimal intervals have seasonal cycles with more
479 summer Sr/Ca values than winter values causing an apparent warm bias. The latter could
480 not be identified for core Totor 1918-1919 values. Nevertheless, the extreme warm
481 anomaly between 1916 to 1921 is most likely related to the change in growth direction
482 associated with an unidentified vital effect. Interestingly, despite the potential influence



483 of vital effects on the trend, the seasonality in this core section was well preserved. This
484 implies that seasonality can be captured robustly while absolute values and trends are
485 potentially biased by vital effects. This adds confidence for the study of seasonality from
486 fossil corals where vital effects are harder to distinguish from true variability due to the
487 lack of SST data for verification.

488 The warm anomalies in the periods 1854-1860, 1936-1941 and 1948-1951 in core
489 Totor are all associated with an orientation of corallites at an angle to the slab surface.
490 Yet, the interval 1936 to 1941 shows a high growth rate and normal seasonality in Sr/Ca
491 for all years and no extreme over-representation of summer versus winter samples. The
492 intervals 1948 to 1951 and 1854 to 1860 both showed reduced growth and seasonality
493 which might have caused apparent warmer winter Sr/Ca values. We also detected areas
494 with warm anomalies for years that predate instrumental data coverage (Tab. 2). The
495 1820's and 1830's likely have a warm bias due to corallites at an angle, disorganized fans
496 and reduced growth rate with more summer values (Tab. 2). Between 1798 and 1816, the
497 orientation is optimal and no bias can be inferred. The years pre-1798 have to be
498 considered with caution since the bottom of the core Totor did show disorganized fans at
499 places and/or suboptimal orientations pointing to likely warm biases (indicated in Figure
500 6).

501 Between 1984 and 2005 (core tops), Sr/Ca trends in cores Totor and Cabri deviate
502 with Totor showing a cooling trend while Cabri shows a strong warming trend (Fig. 7).
503 Our analysis of growth orientation revealed that the corallites in core Totor form parallel,
504 elongated rods of septa for the entire period 1984 to 2005 (Fig. 7) while Cabri does show
505 an optimal orientation of corallites for the core top between 1984 and 2006 (Fig. 7), with



506 the exception of sub-optimal corallites in the period 2000 to 2006. The peculiar structure
507 of the corallites in Totor, at a first glance, would suggest optimal vertical growth of the
508 corallites with the polyps clearly visible from the apex of the core slab. However, this
509 structure is clearly associated with high Sr/Ca ratios and artificially cold SST anomalies.
510 A similar structure of the corallites was found in *Porites lutea* from St. Marie Island off
511 East Madagascar (core STM4 in Grove et al. 2013). Grove et al. (2013) ascribed the
512 Sr/Ca trend difference between cores STM2 and STM4 to changes in coral growth and
513 calcification, yet their results were not conclusive. Re-examination of core STM4
514 revealed that it also forms the parallel-elongated rods of septa in the core top, which was
515 biased towards high Sr/Ca ratios and therefore cold SST anomalies. STM4 also showed
516 low densities in this core top section that agrees with low density in Totor. Inspection of
517 various core sections in Totor and other coral cores revealed that similar elongated rods
518 of septa (not sampled down core) are formed between neighboring growth fans of septa.
519 We suggest that these parallel septa grow very fast in summer and winter, therefore show
520 no clear density contrast with overall low skeletal density. The Sr/Ca seasonality is also
521 strongly enhanced and samples contain a higher number of winter samples that record
522 high Sr/Ca ratios in Totor. Interestingly, the summer Sr/Ca values between cores Totor
523 and Cabri agree rather well between 1984 and 2005 while the winter values in Totor are
524 strongly biased to extreme cold anomalies. We suggest that core tops from *Porites* sp.
525 with similar parallel septa should be avoided for sampling since it can cause a cold bias in
526 Sr/Ca-based SST reconstructions.

527 Overall, our test for sampling biases to a large extend confirms the findings of De
528 Long et al. (2012) and indicates that such analysis should accompany climate



529 reconstructions from coral cores. Our results suggest that a new core needs to be obtained
530 from the Totor colony or other large *Porites* sp. in order to overcome the SST biases
531 identified in the current record. The Cabri coral (>3.5m in height) would be an ideal site
532 since for the period 1945 to 2006 it provided an excellent and largely un-biased record of
533 SST. Yet, the 1907 dead surface was present in three long cores drilled from the Cabri
534 coral at different angles, which could undermine the SST reconstruction for a few
535 decades below the mortality event. The reason for the mortality event could not be
536 determined.

537

538 **6.2 SST trends and large-scale climate teleconnections since 1945**

539 Based on our analysis of corallite orientations, we conclude that core Cabri is
540 most likely the best representation to assess SST trends and interannual variability since
541 1945. Nevertheless, trend estimates in both individual cores and for the composite record
542 need to be interpreted with caution (as indicated in Figure 6).

543 Both, the Cabri and coral composite time series show an increase in SST over the
544 past 60 years (since 1945; Figs. 5 and 6). The Cabri time series recorded a higher SST
545 rise ($1.38 \pm 0.41^\circ\text{C}$) than instrumental data, which ranged between 0.61 to $0.86 \pm 0.15^\circ\text{C}$,
546 and the composite coral record (0.44 ± 0.37). The trend in Cabri agrees with all SST
547 datasets within 2σ , whereby the lower range of uncertainty for the Cabri trend estimates
548 ($\sim 1^\circ\text{C}$) and the upper range for the coral composite ($\sim 0.8^\circ\text{C}$) is in closes agreements to
549 trends from gridded SST datasets. Most of the accelerated warming trend in Cabri
550 resulted from the recent 6 years where the orientation of the corallites was sub-optimal.
551 The composite record agrees with the trend in AT at Rodrigues and marine AT



552 (HadMAT1, HadNMAT2) within 1σ , yet likely underestimates the trend in grid-SST
553 (Fig. 5; Figs. A5, A6). The AT record shows very warm anomalies for the years 1951 to
554 1955 which resulted in a lower long-term trend. The composite record also showed warm
555 years between 1951 and 1955 due to core Totor that indicated warm SST while Cabri
556 followed grid SST with colder temperatures (Fig. 5). The Totor site is a sheltered location
557 with light winds and restricted water movement, with all three having contributed to
558 severe bleaching in 2002 at this site (Hardman et al., 2004, 2008). It could well be that
559 core Totor has at times recorded local SST variations that do not reflect open ocean
560 conditions or those at the more exposed site Cabri. This site-specific, local SST
561 variability might partly explain the high SST anomalies in Totor between 1936 and 1941
562 where the orientation of the corallites did not conclusively accounted for Sr/Ca-SST
563 anomalies. We conclude that the SST trend in Cabri and the coral composite closely
564 follows open ocean grid-SST which both indicate strong warming ($\sim 0.68\text{--}1^\circ\text{C}$) of the
565 south-central Indian Ocean over the past 60 years. Roxy et al. (2014) reported that during
566 1901–2012, the Indian Ocean warm pool warmed by 0.78°C while the western Indian
567 Ocean (5°S – 10°N , 50° – 65°E) experienced anomalous warming of 1.28°C in summer
568 SSTs. Our results for Cabri are therefore not unusual and within the range of observed
569 Indian Ocean SST trends (Annamalei et al., 2005; Alory et al., 2007; Koll Roxy et al.,
570 2014). The strong warming in the southern Indian Ocean trade wind belt could potentially
571 alter the monsoon circulation, especially during the monsoon onset phase in austral
572 autumn (March to May; Annamalei et al., 2005). Both, our coral SST time series and SST
573 products indicate the strongest warming for the March to May season (not shown).
574 Rodrigues station precipitation is strongly positively correlated with SST between March



575 and May. When precipitation is anchored over a warmer SWIO between March and May
576 it can prevent the movements of the ITCZ towards the North and potentially disrupt the
577 Asian monsoon onset (Annamalei et al., 2005).

578 Both the Cabri and coral composite SST reconstructions revealed a clear
579 ENSO/PDO teleconnection pattern for mean annual and austral summer averages with
580 positive correlations across the Indian Ocean resembling the Indian Ocean basin mode
581 pattern (Xie et al., 2016) in response to ENSO and PDO (Fig. 9). Cabri shows the
582 strongest teleconnection pattern, which suggests that this time series is the most reliable
583 between 1945 and 2006 to assess ENSO/PDO impacts on Rodrigues (Figs. A3 to A5).
584 The ENSO/PDO teleconnection was stable for the recent 60 years, yet was strongest
585 between 1971 and 2006 (Fig. 9c,f). The latter period is known for increased occurrence of
586 El Niño events and a switch to a positive PDO phase up to 1999 (McPhaden et al., 2006).
587 These results are in agreement with ENSO/PDO pattern correlations observed in other
588 coral records from the southwestern Indian Ocean (Pfeiffer et al., 2004; Crueger et al.,
589 2009). However, this is the first Indian Ocean coral SST reconstruction that shows a clear
590 relationship with the PDO, while other coral records reflected PDO relationships with
591 rainfall/river runoff (Grove et al., 2013) and salinity/sea level pressure (Crueger et al.,
592 2009; Pfeiffer et al., 204).

593 Coral reefs of Rodrigues escaped the mass coral bleaching event of the 1997–
594 1998 El Niño, yet experienced bleaching in February 2002, March–April 2005 and April–
595 May 2006 (Hardman et al., 2004, 2008). The most severely affected sites with highest
596 coral mortality were located in the north and west of the island with our site Totor located
597 within the zone of most severely affected reefs in 2002, 2005 and 2006 (Hardman et al.,



598 2004, 2008). Our site Cabri showed only 11-30% bleached corals in 2005, yet less severe
599 impacts in 2006 and 2007 and appears less frequently impacted by anomalously high SST
600 during recent El Niño events. Hardman et al. (2008) concluded that coral bleaching at
601 Rodrigues is very patchy and to date most sites appear to be resilient to current El Niño
602 thermal stress events. The relatively large seasonal SST amplitude (6.22°C) and high
603 standard deviation (2.14°C) might serve as buffer to prevent extended periods of thermal
604 stress events during El Niño events. Degree heating weeks for Rodrigues post 1998 rarely
605 exceeded 4 weeks and only in 2002 and 2005 reached 8 weeks at the northern and north-
606 western coral reef sites which have experienced severe thermal stress and are in decline
607 (Hardman et al., 2008). Despite the strong warming trend and El Niño related thermal
608 stress observed in our study, the corals of Rodrigues appear to be a safe haven for coral
609 survival. However, expected levels of future warming in the coming decades will
610 increase thermal stress levels and probably increase coral bleaching and mortality.
611 Rodrigues receives a very limited larval supply suggesting that the reefs rely on larval
612 retention and self-seeding for population recovery. Gilmour et al. (2013) and Graham et
613 al. (2015) showed that isolated reefs with limited larval supply might be the more
614 susceptible to climate change-driven reef degradation, despite escaping many of the
615 stressors impacting continental reef systems. It is therefore most important to reduce local
616 stressors at Rodrigues to provide the corals enough time to bounce back after thermal
617 stress disturbance.

618

619 **7 Conclusions**



620 We reconstruct SST for Rodrigues Island located in the south-central Indian Ocean trade
621 wind belt. Our reconstruction is based on two monthly-resolved coral Sr/Ca records
622 (Totor, Cabri) from Rodrigues Island (63°E, 19°S) that extend to 1781 and 1945,
623 respectively. We identify potential biases in our SST reconstructions associated with the
624 orientation of the corallites and conclude that careful screening for diagenesis and
625 orientation of corallites is of paramount importance to ensure high quality of Sr/Ca-based
626 SST reconstructions. However, our proxy records provide the most reliable SST
627 reconstruction between 1945 and 2006 and for several multi-decadal periods over the past
628 224 years. Reconstructed long-term SST trends are within the range of trends reported
629 from observational SST data for the western Indian Ocean. Furthermore, we identify
630 teleconnections with the ENSO/PDO over the past 60 years, eg. warming of SST during
631 El Niño or positive PDO. Our reconstruction is the first coral proxy record for SST that
632 shows a relationship with the PDO spatial correlation pattern in SST. We suggest that
633 Rodrigues Island is an ideal site to assess SST variations in the southern Indian Ocean
634 trade wind belt and their climatic teleconnection with the ENSO/PDO on longer time
635 scales.

636

637 **8 Acknowledgements**

638 The coral paleoclimate work was supported as part of the SINDOCOM grant
639 under the Dutch NWO program ‘Climate Variability’, grant 854.00034/035. Additional
640 support comes from the NWO ALW project CLIMATCH, grant 820.01.009, and the
641 Western Indian Ocean Marine Science Association through the Marine Science for
642 Management program under grant MASMA/CC/2010/02. We thank the team of



643 SHOALS Rodrigues for their excellent support in fieldwork logistics and in the
644 organization of the research and CITES permits. We would also like to thank the
645 Rodrigues Assembly and the Ministry for Fisheries for granting the research and CITES
646 permits. A Senior Curtin Fellowship in Western Australia, and an Honorary Fellowship
647 with the University of the Witwatersrand, South Africa, supported JZ. Bouke Lacet and
648 Wynanda Koot (VUA) helped cut the core slabs and prepared the thin sections. Janice
649 Lough and Eric Matson (AIMS) provided skilled technical support for coral core
650 densitometry measurements and data processing. We thank Dieter Garbe-Schoenberg for
651 assistance with the ICP-OES measurements.

652

653 **References**

654 Alibert, C. and McCulloch M. T.: Strontium/calcium ratios in modern Porites corals from the
655 Great Barrier Reef as a proxy for sea surface temperature: calibration of the thermometer and
656 monitoring of ENSO, *Paleoceanography*, 12(3), 345-363, 1997.

657

658

659 Alory, G. and Meyers, G.: Warming of the Upper Equatorial Indian Ocean and Changes in the
660 Heat Budget (1960–99), *J. Climate*, 22, 93–113, 2009.

661

662 Annamalai, H., Liu, P. and Xie, S.-P.: Southwest Indian Ocean SST Variability: Its Local
663 Effect and Remote Influence on Asian Monsoons, *Journal of Climate*, 18, 4150-4167, 2005.

664

665 Carricart-Ganivet, J. P. and Barnes D. J.: Densitometry from digitized images of X-
666 radiographs: methodology for measurement of coral skeletal density, *Journal of Experimental*
667 *Marine Biology and Ecology*, 344, 67-72, 2007.

668

669 Charles, C. D., Hunter, D. E. and Fairbanks R. G.: Interaction between the ENSO and the Asian



- 670 Monsoon in a coral record of tropical climate, *Science*, 277, 925-928, 1997.
671
- 672 Cobb, K. M., Charles, C. D. and Hunter D. E.: A central tropical pacific coral demonstrates
673 pacific, Indian, and Atlantic decadal climate connections, *Geophysical Research Letters* 28(11),
674 2209-2212, 2001.
675
- 676 Cole, J. E., Dunbar, R. B., McClanahan, T. R. and Muthiga N. A.: Tropical Pacific forcing of
677 decadal SST variability in the Western Indian Ocean over the past two centuries. *Science* 287,
678 617-619, 2000.
679
- 680 Corrège, T.,: Sea surface temperature and salinity reconstruction from coral geochemical
681 tracers. *Palaeogeog. Palaeoclim. Palaeoeco.*, 232, 408-428, 2006.
682
- 683 Crueger, T., Zinke, J. and Pfeiffer M.: Patterns of Pacific decadal variability recorded by Indian
684 Ocean corals. *International Journal of Earth Sciences* 98, doi:10.007/s00531-00008-00324-
685 00531, 2009.
686
- 687 DeLong, K. L., Quinn, T. M., Taylor, F. W., Shen, C.-C. and Lin, K.: Improving coral-base
688 paleoclimate reconstructions by replicating 350 years of coral Sr/Ca variations,
689 *Palaeogeography, Palaeoclimatology, Palaeoecology*, 373, 6-24, 2013.
690
- 691 DeVilliers, S., Sheng, G.T., Nelson, B.K.: The Sr /Ca-temperature relationship in coralline
692 aragonite: Influence of variability in (Sr/Ca)seawater and skeletal growth parameters,
693 *Geochimica et Cosmochimica Acta*, 58, 197-208, 1994.
694
- 695 Felis, T. and Paetzold, J.: Climate records from corals, In: *Marine Science Frontiers for*
696 *Europe*. Eds.: G. Wefer, F. Lamy and F. Mantoura. Berlin, Heidelberg, New York, Tokyo,
697 Springer, p. 11-27, 2003.
698
- 699 Funk, C., Dettinger, M. D., Michaelsen, J. C., Verdin, J. P., Brown, M. E., Barlow, M. and
700 Hoell, A.: Warming of the Indian Ocean threatens eastern and southern African food security



- 701 but could be mitigated by agricultural development, *Proceedings Nat. Acad. Sci.*, 105(32),
702 11081-11086, 2008.
- 703
- 704 Gagan, M. K., Dunbar, G. B. and Suzuki, A.: The effect of skeletal mass accumulation in
705 *Porites* on coral Sr/Ca and $\delta^{18}\text{O}$ paleothermometry, *Paleoceanography* 27, PA1203,
706 doi:10.1029/2011PA002215, 2012.
- 707
- 708 Gilmour, J.P., Smith, L.D., Heyward, A.J., Baird, A.H., Pratchett, M.S.: Recovery of an
709 isolated coral reef system following severe disturbance, *Science*, 340, 69–71, 2013.
- 710
- 711 Graham, N.A.J., Jennings, S.M., MacNeil, M.A., Mouillot, D., Wilson, S.K.: Predicting
712 climate-driven regime shifts versus rebound potential in coral reefs, *Nature*, 518, 94-97, 2015.
- 713
- 714 Grove, C. A., Kasper, S., Zinke, J., Pfeiffer, M., Garbe-Schönberg, D. and Brummer, G.-J. A.:
715 Confounding effects of coral growth and high SST variability on skeletal Sr/Ca: Implications
716 for coral paleothermometry, *Geochem., Geophys. Geosyst.*, 14, doi:10.1002/ggge.20095, 2013.
- 717
- 718 Grove, C. A., Zinke, J., Peeters, F., Park, W., Scheufen, T., Kasper, S.,
719 Randriamanantsoa, B., McCulloch, M. T. and Brummer, GJA (2013). Madagascar corals
720 reveal multidecadal modulation of rainfall since 1708. *Climate of the Past* 9, 641-656.
- 721
- 722 Hardman, E. R., Meunier, M. S., Turner, J. R., Lynch, T. L., Taylor, M. and Klaus R.: The
723 extent of coral bleaching in Rodrigues, *Journal of Natural History*, 38, 3077-3089, 2004.
- 724
- 725 Hardman, E. R., Stampfli, N. S., Hunt, L., Perrine, S., Perry, A. and Raffin, J. S.: The Impacts
726 of coral bleaching in Rodrigues, Western Indian Ocean, *Atoll Research Bulletin*, 555, DOI:
727 10.5479/si.00775630.555.1, 2008.
- 728
- 729 Helmle, K. P., Dodge, R.E., Swart, P.K., Gledhill, D.K. and Eakin, C.M.: Growth rates of
730 Florida corals from 1937 to 1996 and their response to climate change, *Nat. Commun.*, 2, 215
731 doi: 10.1038/ncomms1222, 2011.



732

733 Hendy, E. J., Gagan, M. K., Lough, J. M., McCulloch, M., and deMenocal P. B.: Impact of
734 skeletal dissolution and secondary aragonite on trace element and isotopic climate proxies in
735 Porites corals, *Paleoceanography*, 22, PA4101, doi:10.1029/2007PA001462, 2007.

736

737 Kaplan, A. *et al.* Analyses of global sea surface temperature 1856-1991, *J. Geophys. Res.*, 103,
738 18567-18589, 1998.

739

740 Kennedy J.J., Rayner, N.A., Smith, R.O., Saunby, M. and Parker, D.E.: Reassessing biases and
741 other uncertainties in sea-surface temperature observations since 1850 part 1: measurement and
742 sampling errors, *J. Geophys. Res.*, 116, D14103, doi:10.1029/2010JD015218, 2011.

743

744 Kent, E.C., Rayner N.A., Berry D.I., Saunby M., Moat B.I., Kennedy J.J., Parker D.E.: Global
745 analysis of night marine air temperature and its uncertainty since 1880: the HadNMAT2
746 Dataset, *Journal of Geophys. Res.*, doi: 10.1002/jgrd.50152, 2013.

747

748 Koll Roxy, M., Ritika, K., Terray, P., Masson, S.: The curious case of Indian Ocean warming,
749 *Journal of Climate* 27, 8501-8509, 2014.

750

751 Lee, S.-K., Park, W., Baringer, M. O., Gordon, A. L., Huber, B. and Liu ,Y.: Pacific origin of
752 the abrupt increase in Indian Ocean heat content during the warming hiatus, *Nature Geoscience*,
753 8, 445-449, 2015.

754

755 Lynch T.L., Meunier, M.S., Hooper, T.E.J., Blais, F.E.I., Raffin, J.S.J, Perrine, S., Félicité, N.,
756 Lisette, J., Grandcourt, J.W.: Annual report of benthos, reef fish and invertebrate surveys for
757 Rodrigues 2002, Shoals Rodrigues report, 30pp, 2002.

758

759 Mantua, N. J., Hare, S. R., Zhang, Y., Wallace, J. M., and Francis, R. C.: A Pacific decadal
760 climate oscillation with impacts on salmon, *Bull. Amer. Meteor. Soc.*, 78, 1069–1079, 1997.

761



762 Mart, Y.: The tectonic setting of the Seychelles, Mascarene and Amirante plateaus in the
763 Western Equatorial Indian ocean, *Marine Geology*, 79, 261-274, 1988.

764

765 McGregor H. V. and Gagan M. K.: Diagenesis and geochemistry of Porites corals from Papua
766 New Guinea: implications for paleoclimate reconstruction, *Geochim. Cosmochim. Acta*, 67,
767 2147–2156, 2003.

768

769 McGregor, H. V. and Abram, N. J.: Images of diagenetic textures in Porites corals from Papua
770 New Guinea and Indonesia, *Geochemistry, Geophysics, Geosystems* 9(10),
771 doi:10.1029/2008GC002093, 2008.

772

773 McPhaden, M. J., Stephen E. Zebiak, S. E., Glantz, M. H.: ENSO as an Integrating Concept in
774 Earth Science, *Science*, 314, 1740-1745, 2006.

775

776 Nakamura, N., Kayanne, H., Iijima, H., McClanahan, T. R., Behera, S. K. and Yamagata, T.:
777 Mode shift in the Indian Ocean climate under global warming stress, *Geophysical Research*
778 *Letters*, 36, L23708, doi:10.1029/2009GL040590, 2009.

779

780 New A. L., Alderson S. G., Smeed D.A., Stansfield K.L.: On the circulation of water masses
781 across the Mascarene Plateau in the South Indian Ocean, *Deep-Sea Research I* 54, 42–74, 2007.

782

783 New A. L., Stansfield, K., Smythe-Wright, D., Smeed D. A., Evans, A. J. and Alderson, S. G.:
784 Physical and biochemical aspects of the flow across the, Mascarene Plateau in the Indian
785 Ocean, *Philosophical Transactions of the Royal Academic Society* 363, 151–168, 2005.

786

787 Paillard, D., Labeyrie, L., Yiou, P.: Macintosh program performs time series analysis. *Eos*
788 *Trans AGU* 77, 379, 1996.

789

790 Pfeiffer, M., Timm, O. and Dullo, W.-C.: Oceanic forcing of interannual and multidecadal
791 climate variability in the southwestern Indian Ocean: Evidence from a 160 year coral isotopic



792 record (La Reunion, 50E, 21S). *Paleoceanography*, 19, PA4006, doi:10.1029/2003PA000964,
793 2004.

794

795 Pfeiffer, M., Timm, O., Dullo, W.-C. and Garbe-Schoenberg, D.: Paired coral Sr/Ca and $\delta^{18}\text{O}$
796 records from the Chagos Archipelago: Late twentieth century warming affects rainfall
797 variability in the tropical Indian Ocean, *Geology*, 34(12), 1069-1072, 2006.

798

799 Pfeiffer, M., Dullo, W.-C., Zinke, J. and Garbe-Schoenberg, D.: Three monthly coral Sr/Ca
800 records from the Chagos Archipelago covering the period of 1950-1995 A.D.: reproducibility
801 and implications for quantitative reconstructions of sea surface temperature variations,
802 *International Journal of Earth Sciences*, 98, doi:10.007/s00531-00008-00326-z, 2009.

803

804 Rayner, N. A., Parker, D. E., Horton, E. B., Folland, C. K., Alexander, L. V., Rowell, D. P.,
805 Kent, E. C. and Kaplan A.: Global analyses of sea surface temperature, sea ice, and night
806 marine air temperature since the late nineteenth century. *Journal of Geophysical Research*
807 **108**(D14), doi:10.1029/2002JD002670, 2003.

808

809 Reynolds, R.W., Rayner, N.A., Smith, T.M., Stokes, D.C., Wang W.: An improved in situ and
810 satellite SST analysis for climate, *Journal of Climate*, 15, 1609–1625, 2002.

811

812 Reynolds, R. W., Smith, T. M., Liu, C., Chelton, D. B., Casey, K. S. and Schlax, M. G.: Daily
813 high-resolution blended analyses for sea surface temperature, *J. of Climate*, 20, 5473-5496,
814 2007.

815

816 Sayani, H. R., Cobb, K. M., Cohen, A. L., Crawford Elliott, W., Nurhati, I. S., Dunbar, R. B.,
817 Rose, K. A., Zaunbrecher, L. K.: Effects of diagenesis on paleoclimate reconstructions from
818 modern and young fossil corals, *Geochimica et Cosmochimica Acta*, 75, 6361–6373, 2011.

819

820 Schott, F.A., McCreary, J.P.: The monsoon circulation of the Indian Ocean, *Progress in*
821 *Oceanography*, 51, 1–123, 2001.

822



- 823 Schrag, D.P.: Rapid analyses of high-precision Sr/Ca ratios in corals and other marine
824 carbonates, *Paleoceanography*, 14, 2, 97-102, 1999.
- 825
- 826 Sepulcre, S., Durand, N., Bard, E.: Mineralogical determination of reef and periplatform
827 carbonates: calibration and implications for paleoceanography and radiochronology, *Global*
828 *Planet Change*, 66(1–2), 1–9, 2009.
- 829
- 830 Smith, T.M., Reynolds, R.W., Peterson, T.C., Lawrimore, J.: Improvements to NOAA’s
831 historical merged land–ocean surface temperature analysis (1880–2006), *J. of Climate*, 21,
832 2283, 2008.
- 833
- 834 Smodej, J., Reuning, L., Wollenberg, U., Zinke, J., Pfeiffer, M. and Kukla, P. A.: Two-
835 dimensional X-ray diffraction as a tool for the rapid, nondestructive detection of low calcite
836 quantities in aragonitic corals, *Geochemistry, Geophysics, Geosystems*, 16,
837 10.1002/2015GC006009, 2015.
- 838
- 839 Tokinaga, H., Xie, S.P., Deser, C., Kosaka, Y., Okumura, Y. M.: Slowdown of the
840 Walker circulation driven by tropical Indo-Pacific warming. *Nature*, 491, 439-444, 2012.
- 841
- 842 Turner, J. and Klaus, R.: Coral reefs of the Mascarenes, Western Indian Ocean, *Philosophical*
843 *transactions of the Royal Academic Society*, 363, 229–250, 2005.
- 844
- 845 van Oldenborgh, G. J., Burgers, G.: Searching for decadal variations in ENSO
846 precipitation teleconnections, *Geophys. Res. Lett.*, 32, L15701, 2005.
- 847
- 848 Woodruff, S.D. *et al.*: ICOADS Release 2.5: Extensions and enhancements to the surface
849 marine meteorological archive, *Int. J. Climatol.*, 31, 951-967, 2011.
- 850
- 851 Xie, S.-P., Kosaka Y., Du Y., Hu K. M., Chowdary J. S., and Huang G.: Indo-western Pacific
852 ocean capacitor and coherent climate anomalies in post-ENSO summer: A review, *Adv. Atmos.*
853 *Sci.*, 33(4), 411–432, 2016.



854

855 Zinke, J., Pfeiffer, M., Park, W., Schneider, B., Reuning, L., Dullo, W.-Chr., Camoin, G. F.,
 856 Mangini, A., Schroeder-Ritzrau, A., Garbe-Schönberg, D. and Davies, G. R.: Seychelles coral
 857 record of changes in sea surface temperature bimodality in the western Indian Ocean from the
 858 Mid-Holocene to the present, *Climate Dynamics*, 43 (3), 689-708, 2014.

859

860 **Appendix A – Coral growth data and comparison to instrumental temperature**

861 **records**

862

863 **Tables**

Core name	GPS position	Species	Water depth (m)	Mean growth rate cm year⁻¹	Mean density g/cm³	Mean Calcification rate g/cm² year⁻¹
Totor	S19°40.237; E63°25.754	<i>Porites</i> <i>sp.</i>	4.0	0.92 (±0.19)	1.128 (±0.11)	1.07 (±0.18)
Cabri	S19°40.030, E63°26.065	<i>Porites</i> <i>lobata</i>	3.0	1.18 (±0.25)	1.36 (±0.12)	1.60 (±0.16)

864 Table 1 - Coral cores with their GPS co-ordinates and depths at low tide, with mean rates
 865 of extension, densities and calcification over the complete length of the individual
 866 records.

867

868

869

870

871

872

873



Section	Year	Orientation	Bias	Notes
1	2005-1987	Sub-optimal	cool	Corallites parallel to surface, yet straight angle; probably like a valley
2	1987-1982	Sub-optimal	cool	Corallites parallel to surface, yet straight angle; probably like a valley
2	1981-1977	Sub-optimal	warm	Corallites at an angle to the surface; oblong corallites
3	1978-1975	Sub-optimal	warm	Corallites at an angle to the surface
3	1974-1958	Optimal	none	Corallites parallel to surface
4A	1958-1952	Sub-optimal	warm	Corallites at an angle to the surface; scallop texture from angles of corallites
4A	1951-1945	Sub-optimal	warm	Corallites at an angle to the surface; 1947-1952 low growth rate; reduced seasonality
4B	1947-1936	Optimal	none	Corallites parallel to surface, 1945-1947 better orientation than in slab 4A
4B	1938-1933	Sub-optimal	none	Corallites at an angle to the surface; 1936-1941 warm anomaly years show normal seasonality and high growth rate
5	1933-1922	Optimal	none	Corallites parallel to surface; 1922-1928 reduced seasonality
6	1921-1915	Sub-optimal	warm	1915-21 warm spikes shows slightly oblong corallites, yet normal seasonality; switch from optimal to sub-optimal orientation
6	1915-1896	Optimal to sub-optimal	none	Corallites mostly parallel to surface, small section with corallites at slight angle;
7	1897-1890	Optimal	none	Corallites parallel to surface
7	1887-1882	Optimal	cool	Diagenesis detected between years 1882-1887
7	1881-1872	Sub-optimal	none	Corallites at an angle to the surface; 1872 close to bioerosion track; 1878-1880 low seasonality, yet no effect
8	1872-1868	Sub-optimal	cool	Corallites at an angle to the surface; some corallites at almost 90° angle; 1868-1872 below bioerosion track; 1867-1871 low seasonality
9	1860-1854	Sub-optimal	warm	Corallites at an angle to the surface; 1854-1858 low seasonality, less winter samples
9	1856-1845	Sub-optimal	warm	Corallites parallel to surface; low seasonality with relatively warm winter samples
9	1844-1831	Optimal	none	Corallites parallel to surface; only 1831-1832 corallites at an angle to surface
10	1830-1827	Sub-optimal	warm	Corallites at an angle to the surface; oblong orientation
10	1826-1823	Disorganised	warm	Corallites rotating at 90° angle; low growth rate, seasonality reduced 1823-1825 with relatively warm winter samples
10	1822-1815	Optimal	none	Corallites parallel to surface; low growth rate; reduced seasonality 1818-1822, yet no effect on SST anomalies
11	1816-1806	Sub-optimal	none	Corallites at an angle to the surface, yet no effect on SST anomalies
11	1807-1798	Sub-optimal	none	Corallites at an angle to the surface in sub-optimal parts; Corallites rotating at 90° angle near terminating fans (not sampled); 3 growth axes with terminating fans in between (not sampled); 1799-1807 regular seasonality
11	1797-1792	Sub-optimal	warm	Corallites at an angle to the surface
12	1795-1792	Disorganised	warm	Corallites rotating at 90° angle; 1792-1791 long year, more summer samples
12	1791-1784	Sub-optimal	warm	Corallites parallel to surface; 1784-1787 Corallites at an angle to the surface; 1789-1794 seasonality distorted
12	1781-1783	Disorganised	warm	Corallites rotating at 90° angle; seasonality slightly distorted, apparently more summer samples

874 Table 2 – Summary of sampling issues detected in core Totor. Unbiased sampling tracks
 875 indicated in bold.



876

Section	Year	Orientation	Bias	Notes
1	2007-2000	Sub-Optimal	warm	Corallites parallel to surface; yet no clear growth fans
1	1999-1992	Optimal	none	Corallites parallel to surface
2	1984-1992	Sub-optimal	none	Corallites at an angle to the surface; oblong corallites
3	1983-1968	Sub-Optimal	none	Corallites parallel to surface; yet no clear growth fan
4	1967-1964	Sub-optimal	none	Corallites at an angle to the surface
5	1963-1958	Optimal	none	Corallites parallel to surface
5	1957-1954	Sub-optimal	none	Corallites at an angle to the surface
5	1953-1945	Optimal	none	Corallites parallel to surface

877

878 Table 3 – Summary of sampling issues detected in core Cabri. Unbiased sampling tracks
 879 indicated in bold.

880

881 **Figure captions**

882 Figure 1 – Map of Rodrigues island with the position of the two corals cores at Totor and
 883 Cabri indicated. The star shows the position of the CTD that collects SST and salinity
 884 data. Polygon indicates the location of the Meteorological Station which records air
 885 temperature, sunshine hours, wind speed and rainfall.

886

887 Figure 2 – Climatology at Rodrigues between 1997 to 2007. A) SST *in situ*, ERSSTv.3
 888 (Smith et al., 2008) and AVHRR SST from NOAA Coral Reef Watch (Reynolds et al.,
 889 2007); b) air temperature and sunshine hours at Rodrigues Meteorological Station (MET);
 890 c) monthly averaged wind speed at MET.

891

892 Figure 3 – a) Time series of monthly (thin solid lines) Sr/Ca anomalies (right Y-axis)
 893 relative to the 1961 to 1990 climatological mean for coral cores Cabri (top), Totor
 894 (middle) and Coral composite (bottom) for the period 1781 to 2006.

895



896 Figure 4 – Reconstructed absolute SST from coral Sr/Ca from cores Totor and Cabri for
897 2002 to 2006 based on calibration with in situ SST from Rodrigues. The uncertainty for
898 single month absolute SST for individual cores Cabri and Totor is 1.23°C and 1.05°C
899 (1σ), respectively. The coral data agree with *in situ* SST within the 1σ uncertainty.

900

901 Figure 5 – Time series of annual mean temperatures anomalies relative to the 1961-1990
902 mean for the coral composite SST, Rodrigues weather station Air temperature (AT),
903 ERSSTv3b, ERSSTv4, HadISST, HadSST3, HadMAT1 and HadNMAT2 for the period
904 1950 to 2006. The uncertainty of mean annual coral Sr/Ca-SST anomalies are indicated
905 by the grey envelope.

906

907 Figure 6 – Annual mean time series of coral time series (red) for a) Cabri, b) Totor and c)
908 the coral composite SST compared to SST reconstructions: ERSSTv3b, ERSSTv4,
909 HadISST, HadSST3, HadMAT1 and HadNMAT2. See legend in a) for colours. For all
910 time series we computed anomalies relative to 1961 to 1990. The uncertainty of mean
911 annual coral Sr/Ca-SST anomalies are indicated by the grey envelope. Potential warm
912 bias in coral SST is indicated by faint red shading, while cool bias by light blue shading.
913 Yellow marks core intervals with diagenesis.

914

915 Figure 7 – a) Monthly interpolated Sr/Ca profiles for cores Cabri (red) and Totor (grey).
916 B) Images of core Totor (coloured blue) with orientation of corallites indicated. Years for
917 core sections indicated on coral slab and grey arrow points to major change in orientation
918 of corallites in core top section of Totor around 1983/84.



919

920 Fig. 8: Thin-section and scanning electron microscope (SEM) images. Thin section
921 photographs are shown in plane- (left) and cross-polarized light (middle). A and B:
922 Excellent preservation of coral skeleton without dissolution or cementation is typical for
923 the corals Totor and Cabri. Small patches of aragonite cements occur in parts of slab 6
924 (C), 7 (D) and 11 (E) of Totor. F (left): A prominent growth break visible in the
925 radiograph of slab 12 of Totor is characterized by abundant microborings and
926 encrustation by coralline red algae. F (middle): The section above the growth break is
927 well preserved. F (right): The coral core Cabri shows excellent preservation, only locally
928 containing aragonitic sediment partially filling pore spaces.

929

930 Figure 9 – Spatial correlation of Cabri Sr/Ca-SST anomalies (relative to 1961-1990) with
931 HadISST (Rayner et al., 2003). January to March austral summer in a) between 1945-
932 2006, b) 1961-1990 and c) 1971-2006. Annual mean correlations in d) between 1945-
933 2006, e) 1961-1990 and f) 1971-2006. Only correlation with $p < 0.05$ are coloured.
934 Computed at knmi climate explorer (van Oldenborgh and Burgers, 2005).

935

936 Figure A1 – Relative changes in coral growth parameters (anomalies relative to 1961-
937 1990) of cores Totor (dark grey; since 1836) and Cabri (light grey; since 1907) versus
938 Rodrigues coral composite SST (black solid line) for period of best geochemical data
939 coverage.

940

941 Figure A2 –Number of SST observations in the grid box surrounding Rodrigues in the
942 ICOADS database. Note the extremely sparse observations even in recent years (van
943 Oldenborgh and Burgers, 2005).

944



945 Figure A3 – Spatial correlations of global austral summer HadISST for 30-year periods
946 with a-f) austral summer coral composite summer SST (January to March) for different
947 30-year periods. Only correlations with $p < 0.05$ coloured. Computed at knmi climate
948 explorer (van Oldenborgh and Burgers, 2005).

949

950 Figure A4 – Spatial correlations of Cabri coral SST with global austral summer HadISST
951 for a-c) 1950 to 1975 (February to May) negative PDO phase (Mantua et al., 1997) and c-
952 d) 1976 to 1999 (January to April) positive PDO phase. Only correlations with $p < 0.05$
953 coloured. Computed at knmi climate explorer (van Oldenborgh and Burgers, 2005).

954 Figure A5 – Spatial correlations of mean annual HadMAT1 air temperature anomalies
955 between 1945 to 2001 relative to 1961-1990 with a) HadISST for Rodrigues, b) coral
956 composite SST and c) Cabri SST. Only correlations with $p < 0.05$ coloured. Computed at
957 knmi climate explorer (van Oldenborgh and Burgers, 2005). Y-axis Latitude, X-axis
958 Longitude.

959

960 Figure A6 – Coral composite monthly SST anomalies relative to 1961-1990 (red)
961 compared to $5^\circ \times 5^\circ$ gridded HadNMAT2 night marine air temperature (blue; Kent et al.,
962 2013). The uncertainty of coral SST based on the regression slope error is indicated by
963 the grey envelope. Note the excellent agreement between the monthly anomalies.
964 Summer (Dec-April) and Winter (June-August) anomalies are correlated with $r = 0.5$,
965 $p < 0.001$ ($N = 56$).

966



967 Figure A7 – X-ray positive print for slabs of core Totor with sampling lines indicated.

968 Blue lines indicate high resolution sampling tracks. Yellow lines superimposed on blue

969 lines indicate sampling at annual resolution for other purposes. Start or end years for each

970 slab indicated.

971

972 Figure A8 - X-ray positive print for slabs of core Cabri with sampling lines (milling

973 holes) indicated. Start or end years for each slab indicated. Note the dead surface before

974 1907 that is most probably related to a past coral bleaching event.

975

976 Table A1 – Statistics of various sea surface temperature (SST) products and air

977 temperature for Rodrigues with 1σ standard deviations in brackets for the period 2002 to

978 2006 (period with *in situ* SST data). STDV = 1σ standard deviation over all years. All

979 units in °C.

980

981 Table A2 - Linear regression of coral Sr/Ca with a) *in situ* SST 2002-2005/6, b)

982 ERSSTv.3 (Smith et al., 2008) 1997-2005/6, c) AVHRR SST NOAA Coral Reef watch

983 data 2000-2005/6 and d) monthly Sr/Ca with AVHRR SST (Reynolds et al., 2007) for the

984 period 1982 to 2005.

985

986

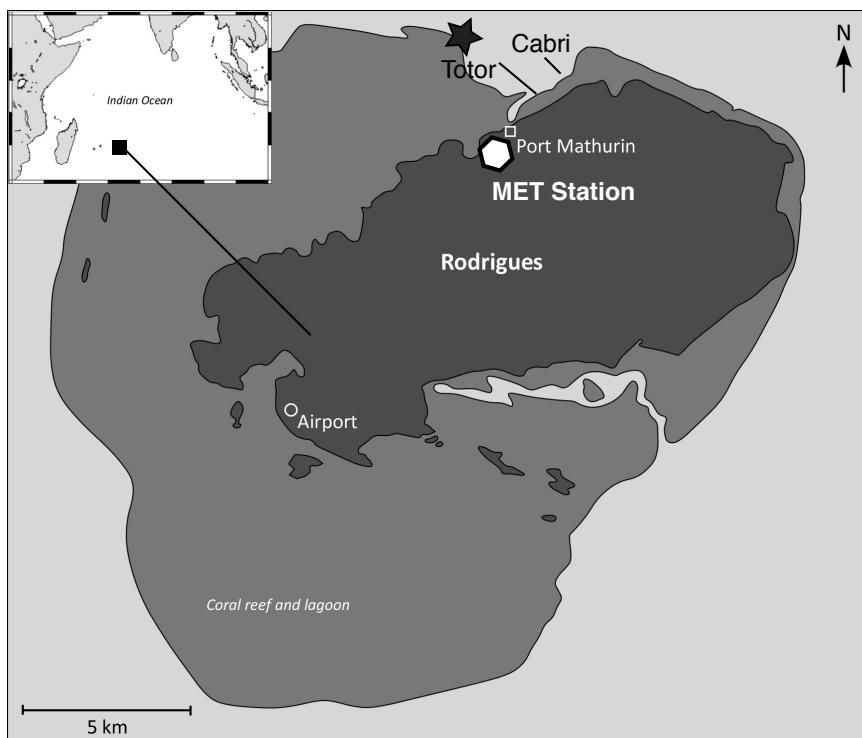
987

988

989



990 **Figures**



991

992 **Figure 1**

993

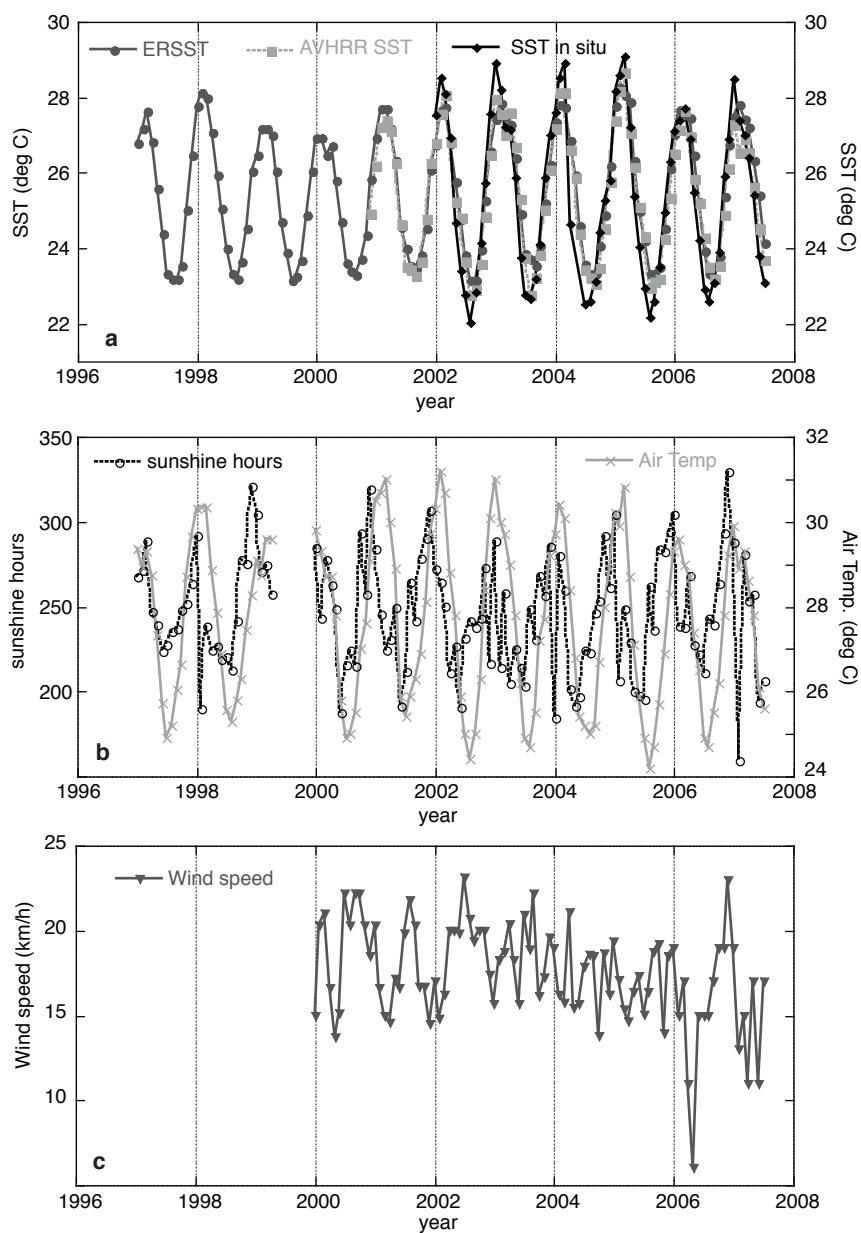
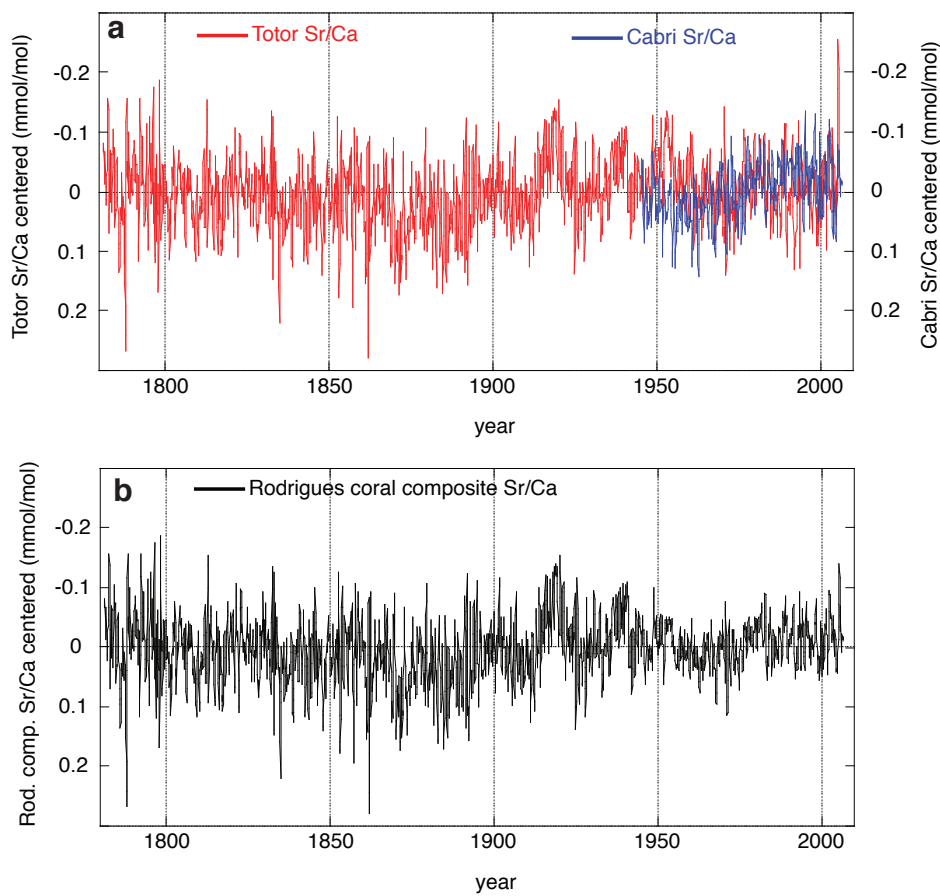


Figure 2

994

995 Figure 2



996

997 Figure 3

998

999

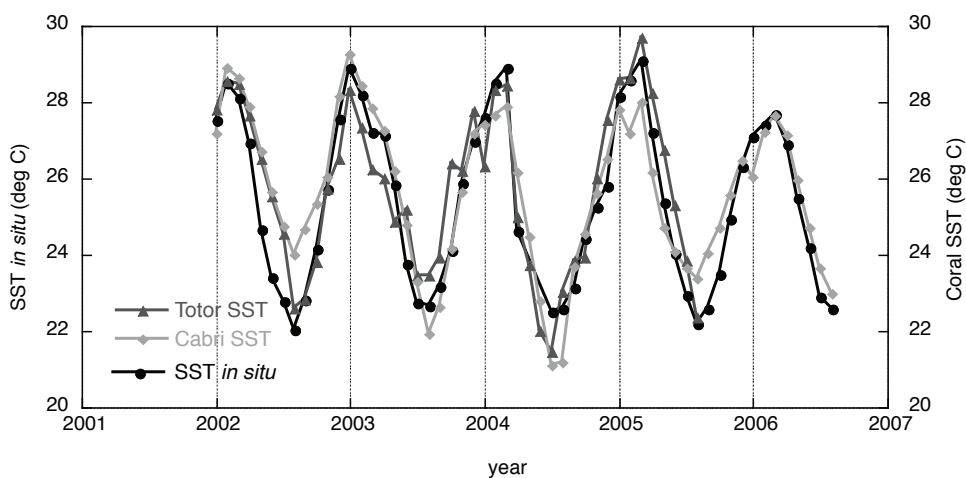
1000

1001

1002

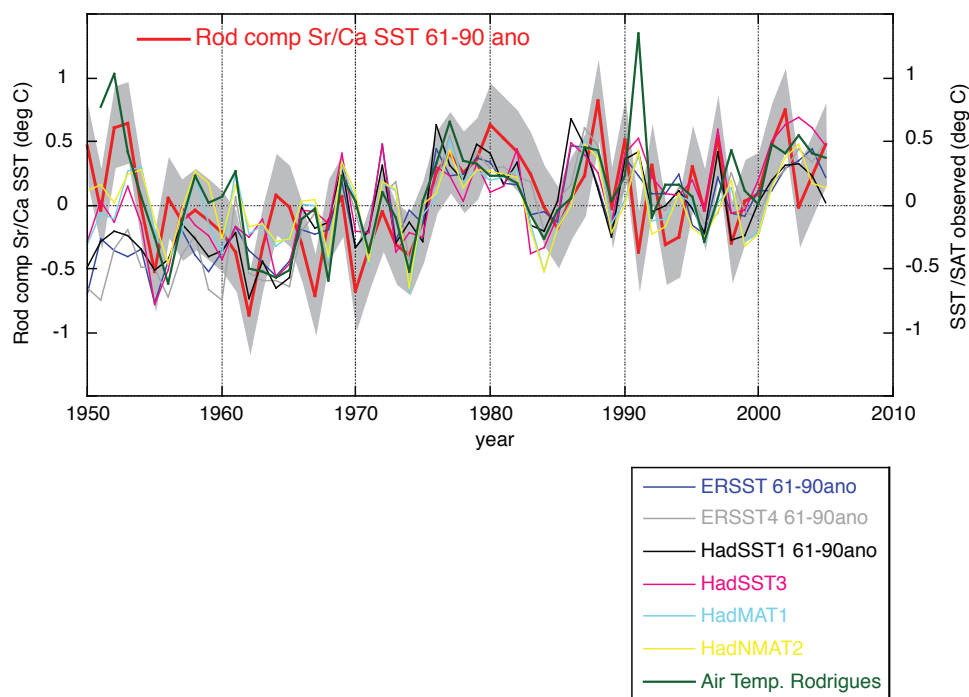
1003

1004



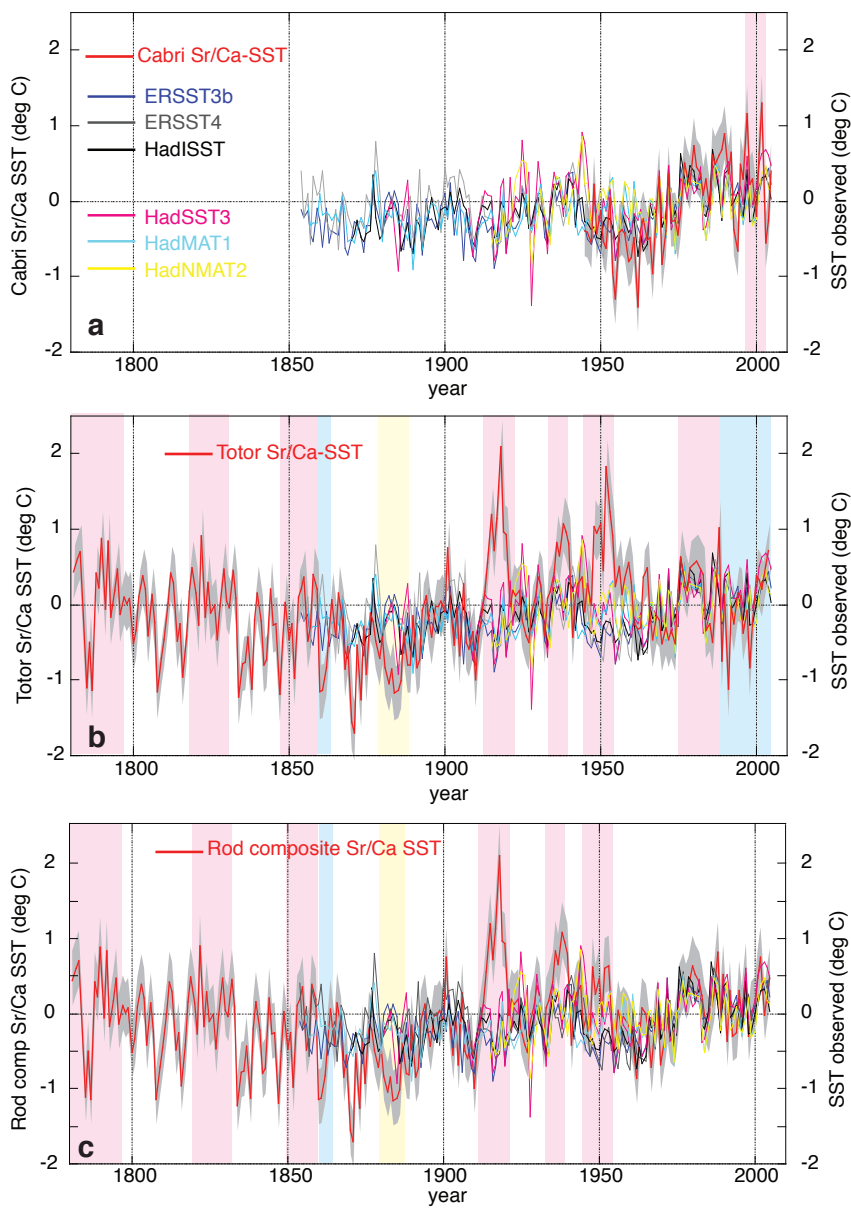
1005

1006 Figure 4



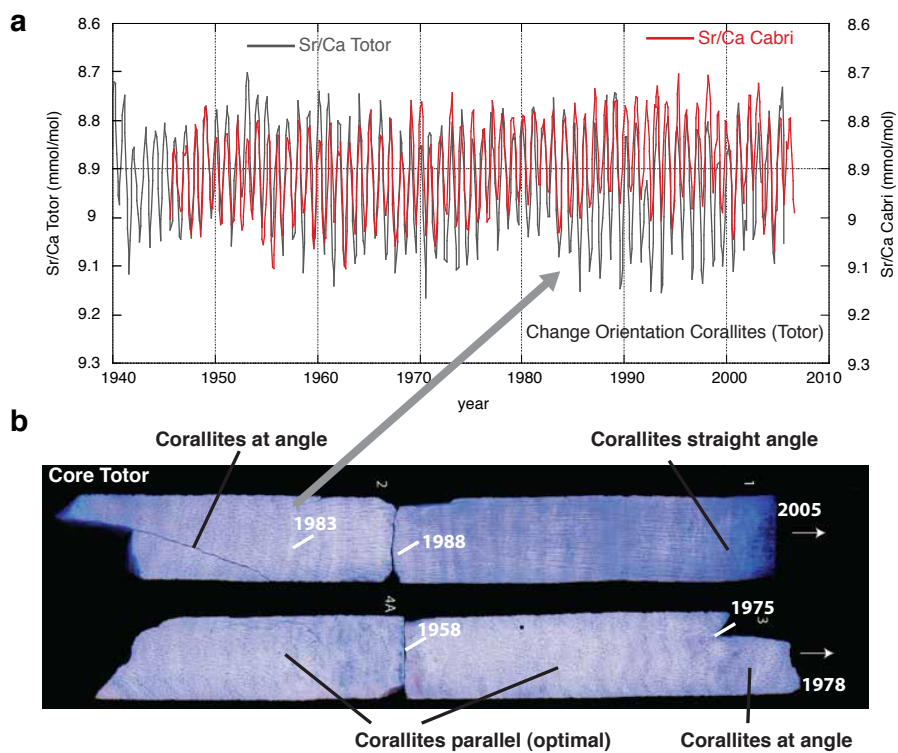
1007

1008 Figure 5



1009

1010 Figure 6



1011

1012 Figure 7

1013

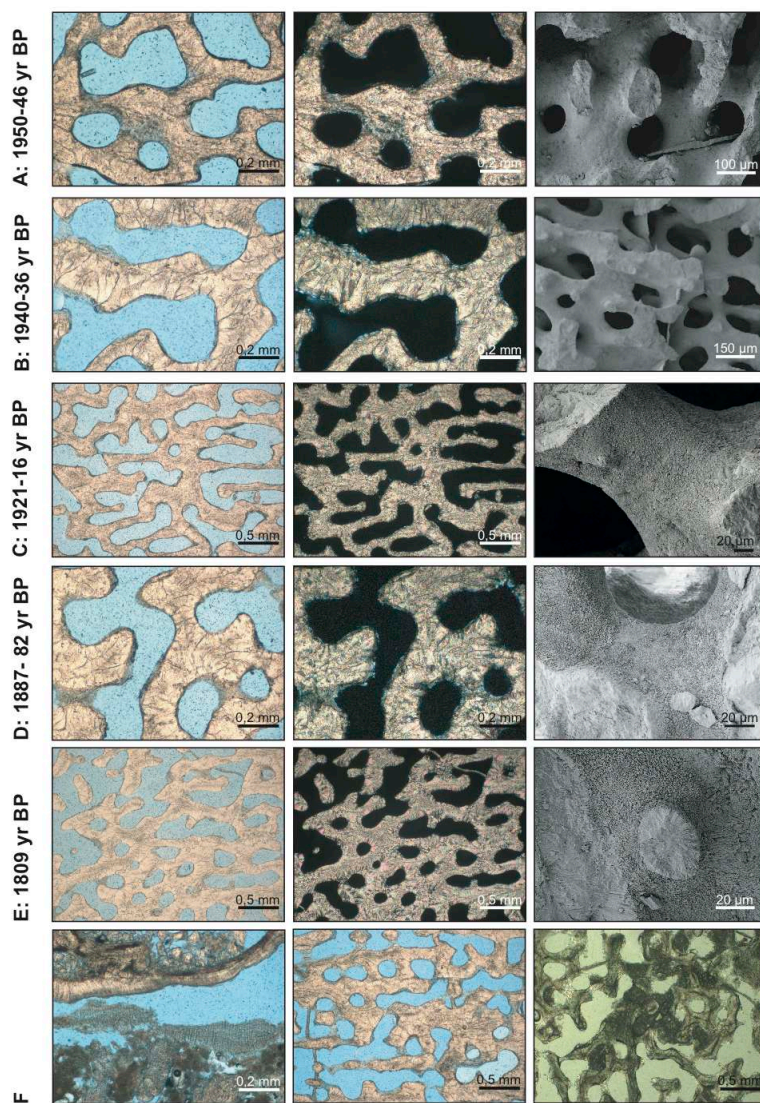
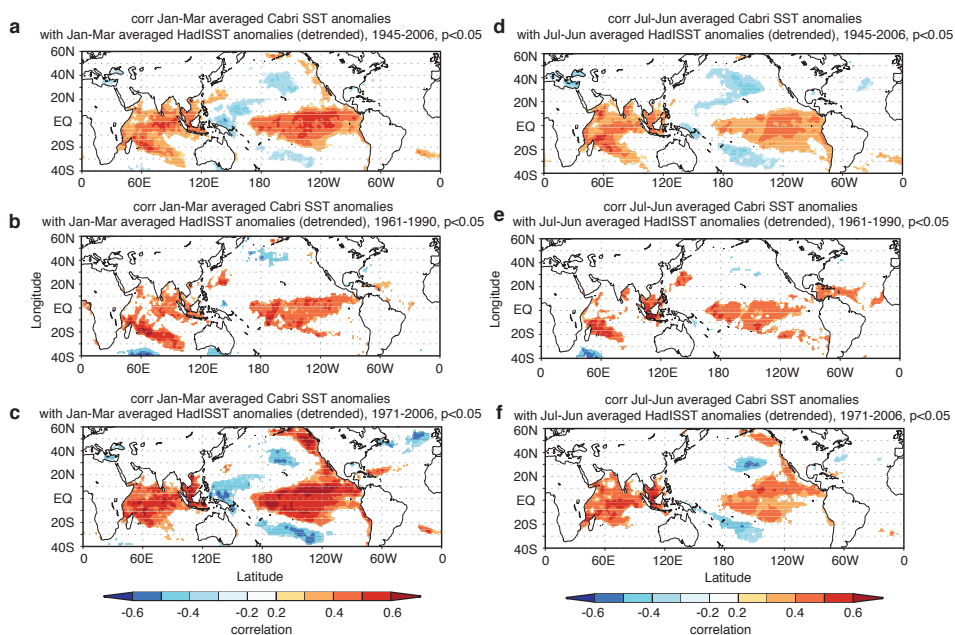


Fig. 8

1014

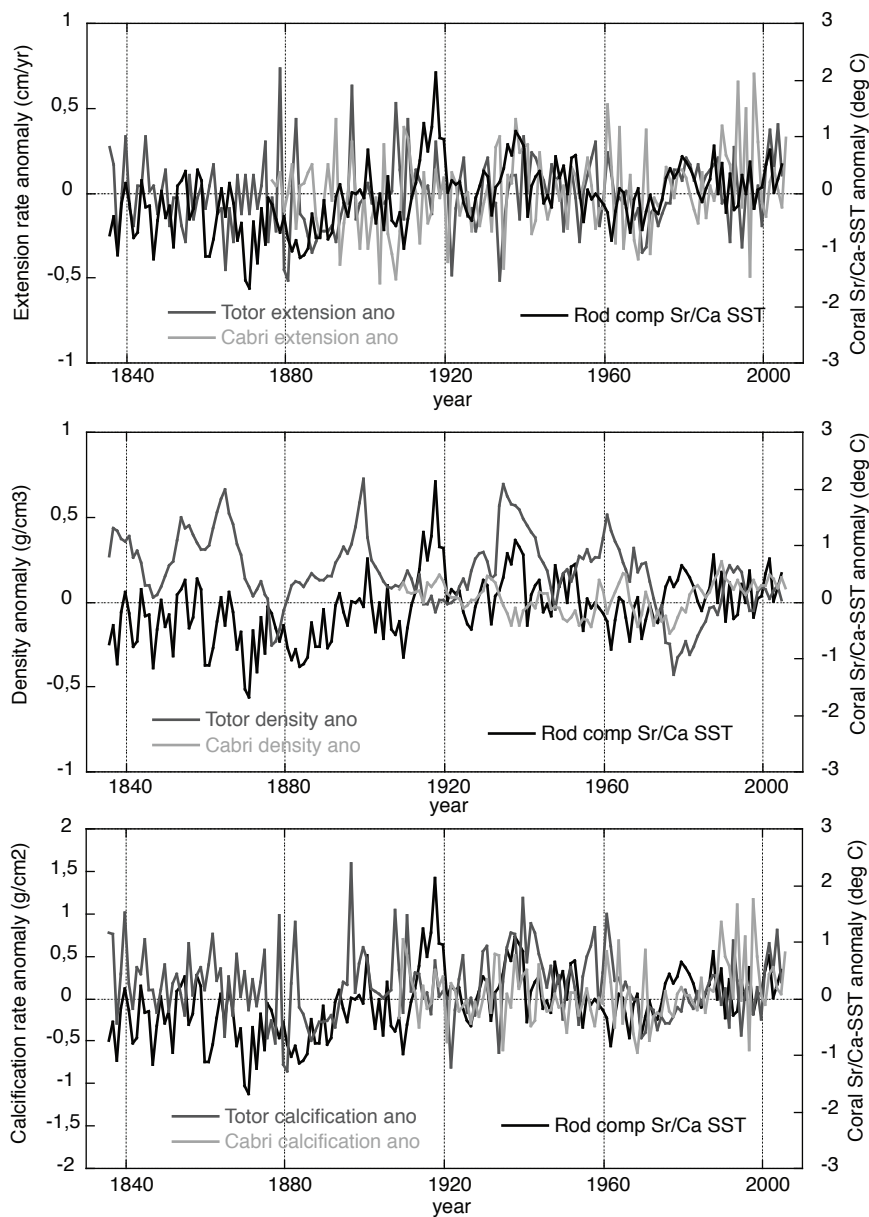
1015 Figure 8



1016

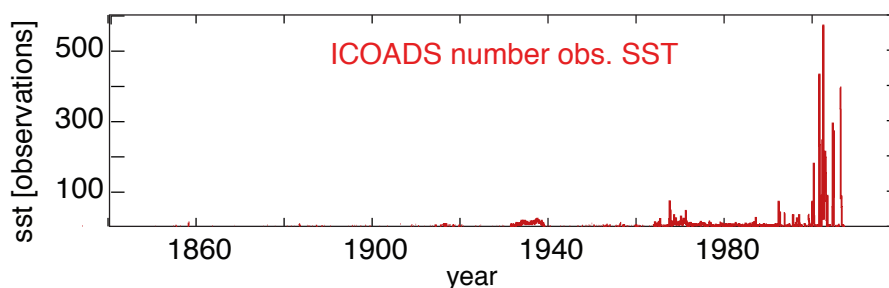
1017 Figure 9

1018



1019

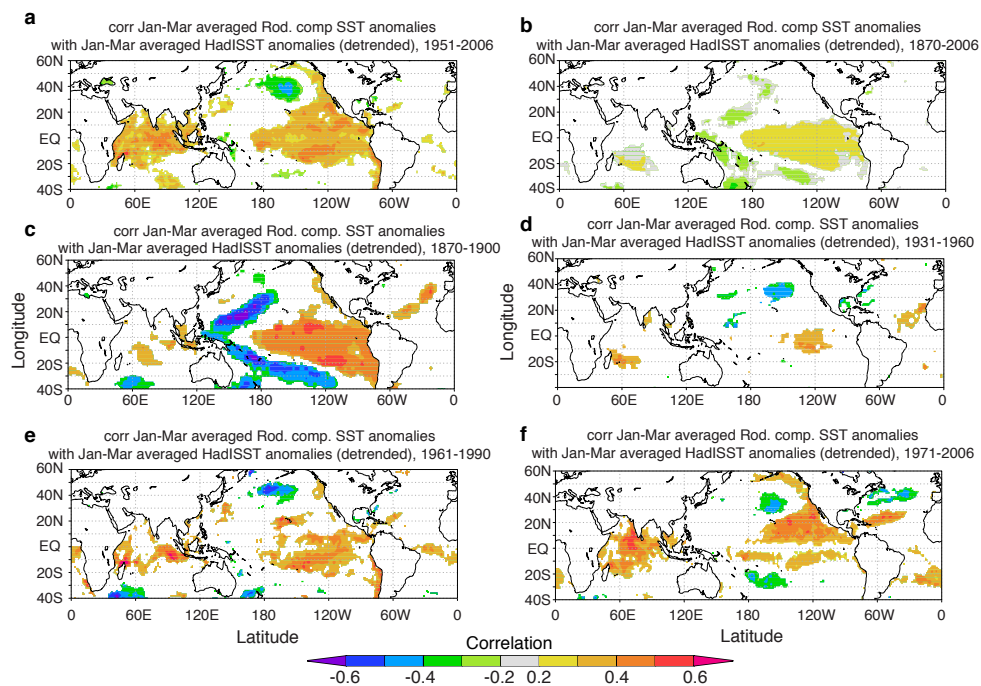
1020 Figure A1



1021

1022 Figure A2

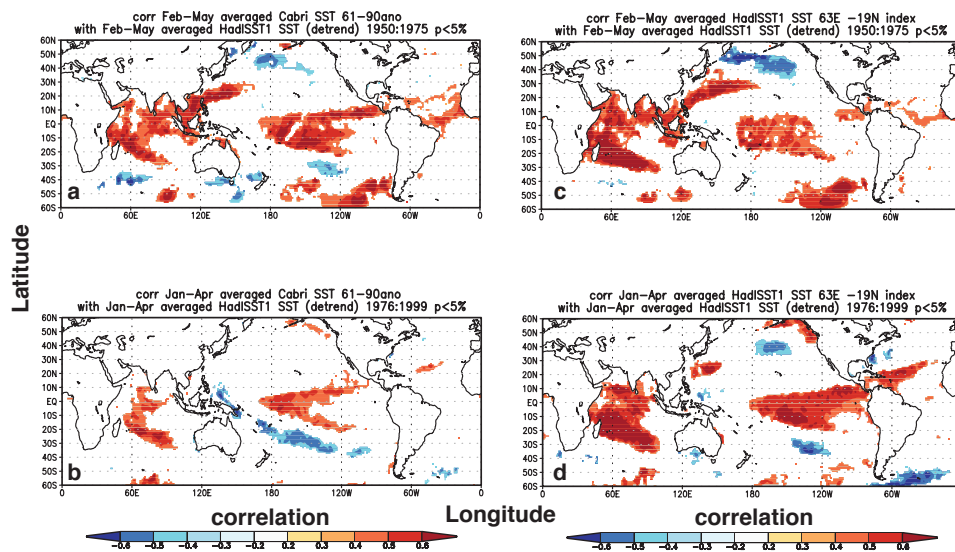
1023



1024

1025 Figure A3

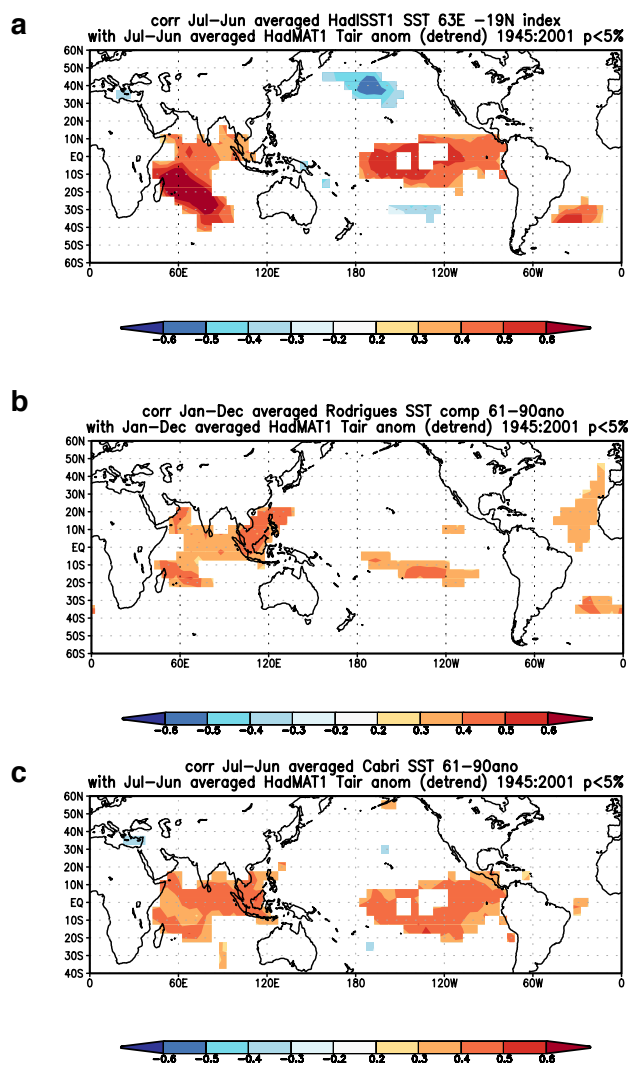
1026



1027

1028 Figure A4

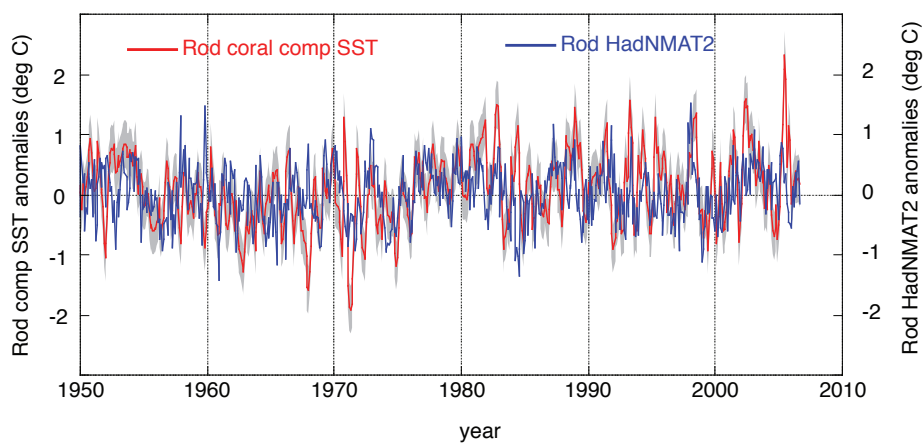
1029



1030

1031 Figure A5

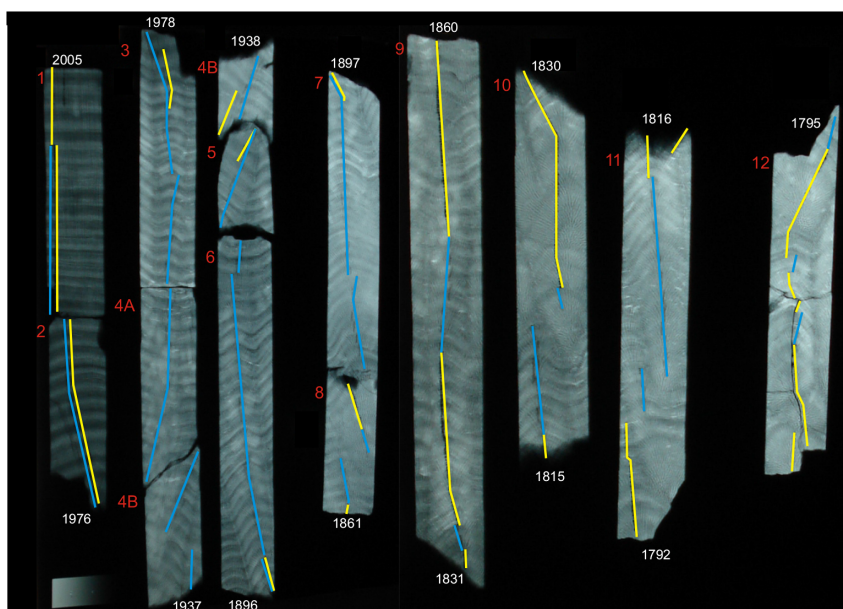
1032



1033

1034 Figure A6

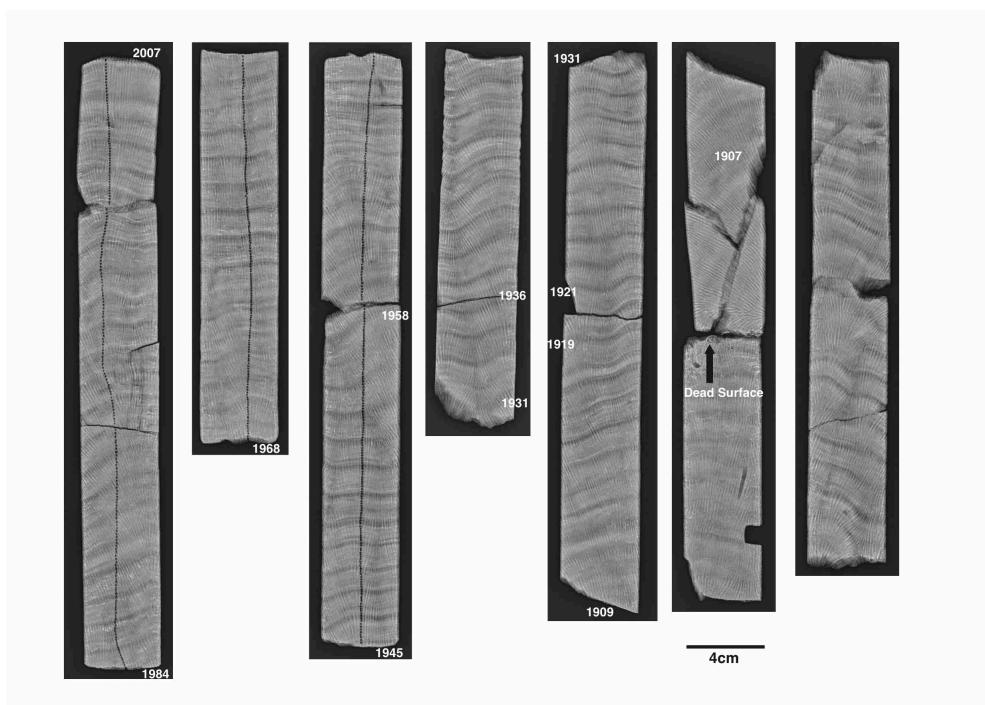
1035



1036

1037 Figure A7

1038



1039

1040 Figure A8

1041

1042

1043

1044

1045

1046

1047

1048

1049

1050



	SST <i>in situ</i>	AVHRR SST	ERSST	Air Temp.
	2002-2006	2002-2006	2002-2006	2002-2006
Mean annual	25.49 (0.24)	25.4 (0.11)	25.57 (0.3)	27.49 (0.31)
Maximum	28.6 (0.5)	28.65 (0.44)	28.29 (0.4)	31.2 (0.62)
Minimum	22.4 (0.27)	22.75 (0.21)	23.15 (0.13)	24.2 (0.44)
Seasonal Range	6.22 (0.68)	5.9 (0.58)	5.14 (0.39)	7.0 (0.79)
STDV	2.14	1.78	1.69	2.07

1051

1052 Table A1 – Statistics of various sea surface temperature (SST) products and air
1053 temperature for Rodrigues with 1σ standard deviations in brackets for the period 2002 to
1054 2006 (period with *in situ* SST data). STDV = 1σ standard deviation over all years. All
1055 units in °C.

1056

1057

1058

1059

1060

1061

1062

1063

1064

1065

1066



(a) Max-Min	Regression equation	r^2	p
Totor	$\text{Sr/Ca} = -0.0439(\pm 0.004) * \text{SST} + 10.032(\pm 0.10)$	0.97	<0.001
Cabri	$\text{Sr/Ca} = -0.0384(\pm 0.005) * \text{SST} + 9.861(\pm 0.12)$	0.89	<0.001
(b) Max-Min			
Totor	$\text{Sr/Ca} = -0.0638(\pm 0.004) * \text{SST} + 10.566(\pm 0.09)$	0.95	<0.001
Cabri	$\text{Sr/Ca} = -0.0507(\pm 0.004) * \text{SST} + 10.179(\pm 0.10)$	0.90	<0.001
(c) Max-Min			
Totor	$\text{Sr/Ca} = -0.0531(\pm 0.004) * \text{SST} + 10.271(\pm 0.11)$	0.96	<0.001
Cabri	$\text{Sr/Ca} = -0.0441(\pm 0.005) * \text{SST} + 10.012(\pm 0.13)$	0.88	<0.001
(d) Monthly			
Totor	$\text{Sr/Ca} = -0.0522(\pm 0.003) * \text{SST} + 10.272(\pm 0.08)$	0.79	<0.001
Cabri	$\text{Sr/Ca} = -0.0419(\pm 0.003) * \text{SST} + 9.95(\pm 0.07)$	0.87	<0.001

1067

1068 Table A2 - Linear regression of coral Sr/Ca with a) *in situ* SST 2002-2005/6, b)

1069 ERSSTv.3 1997-2005/6, c) AVHRR SST NOAA Coral Reef watch data 2000-2005/6 and

1070 d) monthly Sr/Ca with AVHRR SST for the period 1982 to 2005.